Multiphase flow with CO2 as the displacing phase: digital rock, laboratory, and upscaled analysis

Sušilović, Nikolina

Master's thesis / Diplomski rad

2023

Degree Grantor / Ustanova koja je dodijelila akademski / stručni stupanj: **University of Zagreb, Faculty of Mining, Geology and Petroleum Engineering / Sveučilište u Zagrebu, Rudarsko-geološko-naftni fakultet**

Permanent link / Trajna poveznica: https://urn.nsk.hr/urn:nbn:hr:169:108638

Rights / Prava: In copyright/Zaštićeno autorskim pravom.

Download date / Datum preuzimanja: **2024-12-25**

Repository / Repozitorij:

Faculty of Mining, Geology and Petroleum Engineering Repository, University of Zagreb

SVEUČILIŠTE U ZAGREBU

RUDARSKO-GEOLOŠKO-NAFTNI FAKULTET

Diplomski studij naftnog rudarstva

MULTIPHASE FLOW WITH CO_2 AS THE DISPLACING PHASE: DIGITAL ROCK, LABORATORY, AND UPSCALED ANALYSIS

Master's Thesis

Nikolina Sušilović

N381

Zagreb, 2023.

Sveučilište u Zagrebu $\qquad$ Diplomski rad

Rudarsko-geološko-naftni fakultet

VIŠEFAZNI PROTOK S CO2 KAO ISTISKUJUĆOM FAZOM: ANALIZA DIGITALNE STIJENE, LABORATORIJSKA ANALIZA I SKALIRANJE

Nikolina Sušilović

Diplomski rad izrađen: Sveučilište u Zagrebu
                        Rudarsko-geološko-naftni fakultet
                        Zavod za naftno-plinsko inženjerstvo i energetiku
                        Pierottijeva 6, 10000 Zagreb

Sažetak

Migracija oblaka CO_2 modelirana je na razini ležišta. Točnost modela uvelike ovisi o geološkom modelu i parametrima poroznog medija, kao što su poroznost, relativna propusnost i odnosi kapilarnog tlaka. Digitalni alati za analizu stijene, uključujući mikrotomografiju i modeliranje mreže pora, omogućili su analizu protoka u poroznim medijima i poboljšali razumijevanje višefaznog protoka u sustavu CO_2-voda. U kombinaciji s posebnom analizom jezgre u laboratoriju (SCAL), provođenjem eksperimenta ustaljenog protoka, rezultati su povezani i korelirani kako bi se osigurali ulazni podatci za numeričku simulaciju utiskivanja CO_2. Rezultati simulacije su dokazali da se 250 godina nakon utiskivanja oblak kreće sve dok ne dosegne vrh strukture. Dosljednost parametara na svim skalama pokazuje potencijal ovog pristupa skaliranja na više razine.

Ključne riječi: višefazni protok, CO_2-voda relativna propusnost, kapilarni tlak, skaliranje na više razine, modeliranje na razini pora, mikrotomografija, utiskivanje CO_2

Diplomski rad sadrži: 59 stranica, 41 sliku, 7 tablica, 2 priloga i 36 referenci

Jezik izvornika: Engleski

Diplomski rad pohranjen: Knjižnica Rudarsko-geološko-naftnog fakulteta
                          Pierottijeva 6, 10000 Zagreb
Mentor: Dr. sc. Domagoj Vulin, redoviti profesor RGNF-a
Pomoć pri izradi: Marko Gaćina, mag. naft. rud.

Ocjenjivači: Dr. sc. Domagoj Vulin, redoviti profesor RGNF-a
              Dr. sc. Karolina Novak Mavar, docentica RGNF-a
              Dr. sc. Vladislav Brkić, izvanredni profesor RGNF-a

Datum obrane: 24.02.2023., Rudarsko-geološko-naftni fakultet, Sveučilište u Zagrebu

MULTIPHASE FLOW WITH CO_2 AS THE DISPLACING PHASE: DIGITAL ROCK, LABORATORY, AND UPSCALED ANALYSIS

Nikolina Sušilović

Thesis completed at: University of Zagreb
                         Faculty of Mining, Geology and Petroleum Engineering
                         Department of Petroleum and Gas Engineering and Energy
                         Pierottijeva 6, 10000 Zagreb

Abstract

CO_2 plume migration was modeled at the reservoir scale. The accuracy of the model highly depends on the geological model and porous media parameters, such as porosity, relative permeability, and capillary pressure relationships. Digital rock tool analysis, including microtomography and pore network modeling, provided the analysis of the flow in porous media and improved understanding of a multiphase flow in CO_2-water system. In combination with special core analysis in a laboratory, conducting a steady-state experiment, results were correlated and smoothed to provide an input for numerical simulation of CO_2 injection. Simulation results have proved that 250 years after the injection, plume moves until it reaches the top of the structure. The consistency of parameters on all scales, shows a potential of this upscaling approach.

Key words: multiphase flow, CO_2-brine relative permeability, capillary pressure, upscaling, pore-scale modeling, microtomography, CO_2 injection

Thesis contains: 59 pages, 41 figures, 7 tables, 2 appendices and 36 references
Original in: English

Archived in: Library of Faculty of Mining, Geology and Petroleum Engineering
                          Pierottijeva 6, 10000 Zagreb
Supervisor: Full Professor Domagoj Vulin, PhD
Co-mentor: Marko Gaćina, MS Petroleum Engineering.
Reviewers: Full Professor Domagoj Vulin, PhD
                          Assistant Professor Karolina Novak Mavar, PhD
                          Associate Professor Vladislav Brkić, PhD

Defence date: February 24, 2023, Faculty of Mining, Geology and Petroleum Engineering, University of Zagreb

Table of Contents

I. LIST OF FIGURES

II.   LIST OF TABLES

III. LIST OF UNITS

Label	Unit of measurement	Label explanation
D_b	m	Euclidean distance of a specific pixel
x_i, y_i	m	White pixel
x_b, y_b	m	Black pixel
∂Sw	-	Partial derivative of water saturation
∂t	-	Partial derivative of time
Camera stage mode	°	Number of degrees at which the camera scans
Projection increment	°	Increment of degrees at which the camera scans
$N_{projections}$	-	Number of projections
$L_{scanned\ object}$	mm	Length of the sacnned object
N_{pixels}	-	Number of pixels
resolution	μm	Size of the pixels
σ, IFT	N/m	Interfacial tension
Θ	°	Contact angle
γ	kg/m^3	Density
μ	Pa·s	Viscosity
S_{pore}	-	Pore saturation at the limit
S_{throat}	-	Throat saturation at the limit
$V_{pore@pore\ mask}$	m^3	Pore volume at the limit
$V_{throat@throat\ masks}$	m^3	Throat volume at the limit
V_{pore}	m^3	Pore volume
V_{throat}	m^3	Throat volume

$\mathbf{V_{bulk}}$	m^3	Sum of pore and throat volumes
$\mathbf{S}$	-	Saturation point
$\mathbf{K_{rphase}}$	-	Phase relative permeability
$\mathbf{K_{ephase}}$	-	Phase effective permeability
$\mathbf{K_{abs}}$	mD	Absolute permeability
$\mathbf{Q_{e\text{-}phase}}$	m^3/s	Flow rate of one phase in multiphase flow
$\mathbf{Q_{abs\text{-}phase}}$	m^3/s	Single phase flow rate
$\mathbf{Pc}$	Pa	Capillary pressure
$\mathbf{r}$	m	Pore or throat radius
$\mathbf{Q}$	m^3/s	Inlet flow rate
$\mathbf{A_{sample}}$	m^2	Area of the sample
$\mathbf{L_{sample}}$	m	Length of the sample
$\mathbf{N_{voxel}}$	-	Number of voxels
$\mathbf{\Phi}$	%	Porosity
$\mathbf{CT_{xy}}$		CT number
$\mathbf{S_w}$	-	Water saturation
$\mathbf{f_w}$	-	Fractional flow of water
$\mathbf{Ca}$	-	Capillary number
$\mathbf{F_{viscous}, F_{capillary}}$	N	Viscous forces, Capillary forces
$\mathbf{k_{rg}, k_{rw}}$	-	Gas and water relative permeability
$\mathbf{\Delta P^{nw}, \Delta P^w}$	Pa	Non-wetting and wetting phase pressure drop
$\mathbf{k_w}$	mD	Effective water permeability
$\mathbf{S_{wr}}$	-	Residual water saturation
$\mathbf{n_g, n_w}$	-	Corey exponents

d_w	cm	Well diameter
H_{ef}	m	Effective formation height
k_x, k_y	mD	Permeability in x and y direction
c_f	bar^{-1}	Rock compressibility
h_{ref}	m	Datum depth
S_{gc}	-	Critical water saturation
k_{rg_cw}, k_{rw_gc}	-	Water and gas relative permeability endpoints
k_v, k_h	mD	Verical and horizontal permeability
pic	%	Plume increase coefficient
r_{pmax}	m	Maximum plume radius from injection well
p_{mr}	m/year	Plume migration rate

IV.   LIST OF ABBREVIATIONS

ACTNUM – key word for ECLIPSE input format (inactive cells)

CMOS – Complementary Metal Oxide Semiconductor

CO_2 – Carbon Dioxide

CO2STORE – simulation option for CO_2 storage

CT – Computer Tomography

DNS – Direct numerical simulation

DRP – Digital Rock Physics

FGIT – field gas injected total, sm^3

FWIP – Field water in place

ID – Inside diameter

IP – Invasion Percolation

OD – Outside diameter

NaCl – Natrium Chloride

NIST – National Institute of Standards and Technology

MIP – Mercury Intrusion Porosimetry

PNM – Pore Network Modeling

p-T – Pressure, temperature

PV – Pore volume

RESV – simulation control mode for constant reservoir volume rate

SCAL – Special Core Analysis

SNOW – Subnetwork of the Oversegmented Watershed

S/N – Signal to noise ratio

SS – Steady state

TIFF – Tag Image File Format

XRM – X-Ray Microscopy

2D – Two dimensional

3D – Three dimenisonal

1. INTRODUCTION

CO_2 injection in geological formations is a necessary method of reducing CO_2 emissions (i.e. the only large-scale CO_2 removal method), which necessitates the injection of supercritical CO_2 into deep sedimentary strata for long-term storage. Potential storage sites include deep saline aquifers and depleted hydrocarbon reservoirs. Deep saline aquifers are more suitable choices due to their size and if, selected appropriately, the required permeability and porosity values. Injecting CO_2 into the reservoir increases pressure and (to a certain degree) displaces formation water (brine), resulting in a CO_2 plume, which is a highly CO_2-saturated zone visible by monitoring systems and foreseeable by known reservoir engineering methods. Multiphase flow of CO_2 and brine is affected significantly by the relative permeability and the combination of viscous, capillary and gravity forces in which relative permeability determines the displacement efficiency, CO_2 saturation and injection rate (Jeong et al., 2021). As relative permeability changes with saturation, it is directly related to injectivity, which is one of the most important technological parameters, because it determines the injection pressure and capacity to inject CO_2 within a given time period. The advantage is that CO_2 relative permeability (and thus injectivity) increases with the amount of injected CO_2 (i.e. with CO_2 saturation), as opposed to local near-wellbore pressure increase (which acts against injectivity).

Carbon capture and storage (CCS) has been a topic of many various studies from *coreflooding* tests, numerical simulations to field applications. Several studies focus on the relative permeabilities in a CO_2-brine system in which they estimate of this system to oil-water system, for simplicity. Although, properties of the CO_2 phase differ considerably from the oil phase, the CO2-brine system has high interfacial tension and low viscosity ratio (Jeong et al., 2021).

Reservoir models are used to guide the development and injection of CO2 into deep aquifers, and their accuracy depends on analysis tool which predict fluid flow. Proper multiphase flow modeling is performed in the laboratory using a special core analysis (SCAL), which is a time-consuming but provides high-quality data. The alternative is to utilize Digital Rock Physics (DRP), which involves extensive numerical analysis of the core on a computer. DRP also enables the reinterpretation of previously recorded images or the examination of a rock that could not be prepared as core-plugs for SCAL.

The development of such rock imaging tools, such as Pore network Modeling (PNM), improved understanding of the flow in porous media. Suitable descriptions of fluid flow models through porous media depend on parameters, such as porosity, relative permeability and capillary pressure relationships. The advantage is that it is publicly available and saves time and costs at the expense of losing information. Pore network is extracted from a micro-resolution segmented image of the rock's pore structure obtained by microtomography. In this work, OpenPNM and PoreSpy open-source packages are used to extract the pore network and predict relative permeabilities, capillary pressure and calculate absolute permeability of a sandstone core plug scanned with a microCT (Mahdiabad, 2020).

Based on detailed information of a pore and core scale fluid model, which are inputs for a reservoir scale, numerical simulations are obtained. They predict the migration of the CO_2 plume in the subsurface, design CO_2 injection rates and monitor data. A prerequisite for regulatory processes of implementing CO_2 storage projects, is the ability to estimate the migration of a CO_2 plume. Additionally, identifying potential well placements, faults or fractures that may cause leakages. Supercritical CO_2 is denser than brine at storage reservoir temperatures and pressures. Consequently, buoyancy forces are increased and cause the CO_2 to mix with the brine simultaneously dissolving in brine. Viscous forces are large at the injection well, but decrease radially. Residual CO_2 that didn't dissolve in the brine or migrate upwards in a plume, gets trapped in pore. Capillary entry pressures are high in low permeability rocks, creating barriers in heterogeneous rocks ratio (Jeong et al., 2021).

To better understand these effects, in this work, upscaling approach is applied to obtain as much accurate parameters and their relationships using various experimental and digital methods.

2. THEORETICAL BACKGROUND

Providing theoretical background on microtomography, pore network modelling and upscaling approach is important to understand the terminology and methods used in this study.

2.1. Microtomography

Modern imaging techniques are developed through obtaining three-dimensional reconstructions from a set of two-dimensional projections taken at different angles. The sample is rotated, while the absorption of X-rays is recorded and used to reconstruct 3D images of rocks and fluids. Today's approach to image the pore space is to use a microCT scanner, as a laboratory instrument, where the image resolution is primarily determined by the proximity of the rock sample to the beam source (Blunt et al., 2013).

Micro-computed tomography (microCT) or X-Ray Microscopy (XRM) is X-ray imaging in 3D, the same method used in clinical CT scans, but on a small scale with massively increased resolution. It is 3D microscopy that images the internal structure of objects in a non-destructive manner. When X-rays pass through an object the intensity is reduced by absorption proportional to the average atomic number along the trajectory (Figure 2-1.) (Bruker, 2023). It is used for studying all types of samples from 1 mm to 20 cm in diameter and full drill cores. Applications are found in all areas of geoscience, including oil and gas, to image and analyze: porosity, microstructure, composition and 3D mineral distribution. Multi-scale analysis and dynamic processes (fluid motion, multi-phase flow) are also developed (Bluescientific, 2021). The main factors that determine the resolution are sample size, beam quality, detector specifications and specifically, proximity of the sample to the beam. At present, microCT scanners produce images of $1000^3 - 2000^3$ voxels. To produce a representative sample, the cores require a few mm across, to obtain a resolution of a few microns (Blunt et al., 2013). A voxel is the smallest element of volume division in a 3D digital image. A voxel represents a 3D pixel, and its dimensions are limited by the quality of the equipment, i.e. the resolution of the 3D imaging device.
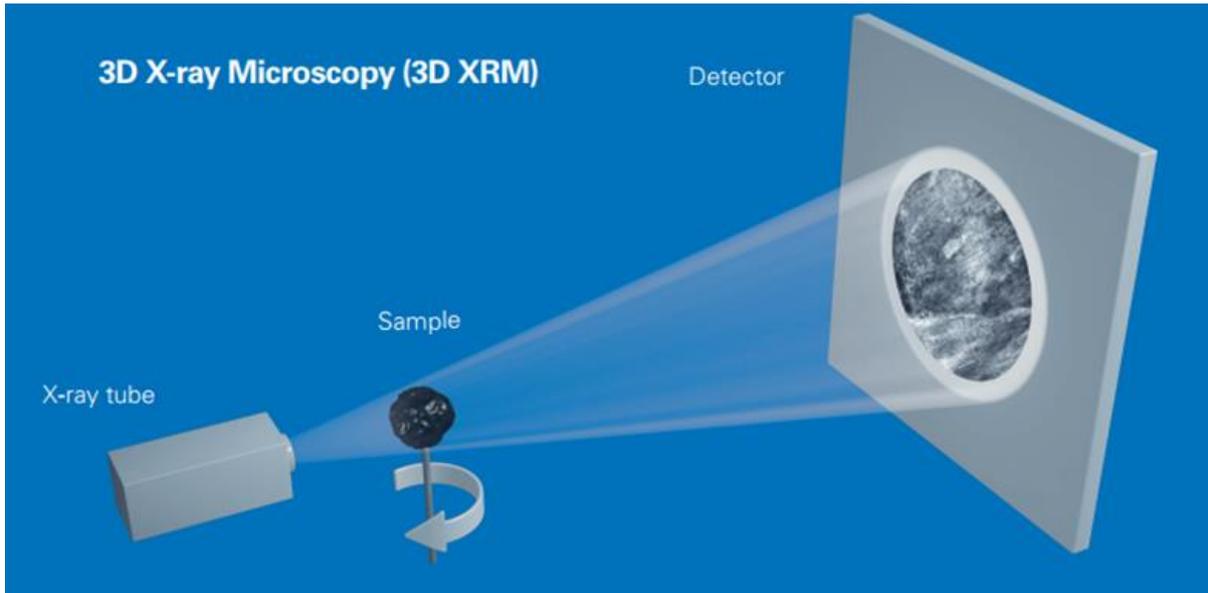
Figure 2-1. 3D X-ray Microscopy (Bruker, 2023)

Bruker's microCT scan contains a variable detector to perform the best scan of all size samples. In Figure 2-2., the smallest sample sits closest to the X-ray source, to obtain micro resolution.
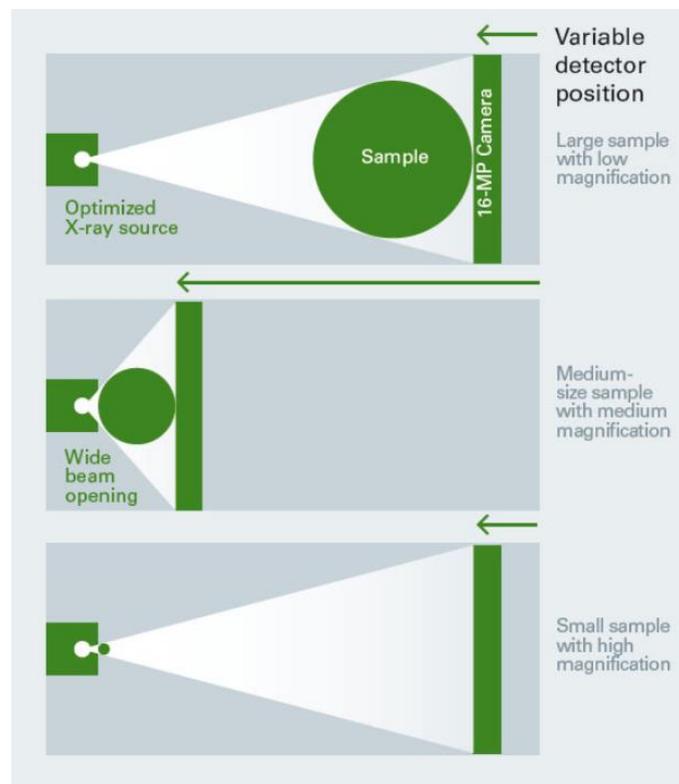

Figure 2-2. Scanning of three sample sizes with variable detector positions (Bruker, 2023)

2.2. Pore Network Modelling

There are two approaches to calculate porous properties. The first is a direct approach that takes into account the geometry of the porous media. This technique is expensive and computationally very demanding (Blunt et al., 2013). Another method is pore network modelling, in which the pore network is extracted as a stick and ball network (Mahdiabad, 2020).

Direct numerical simulation (DNS) is a particle-based technique that simulates the motion and collision of the particles in the grid, which involves an approximation of the Navier-Stokes equations. The method is suited for computing single-phase flow properties, such as permeability and dispersion coefficients, on porous media images. While there are additional techniques that are designed to study capillary-controlled flow where viscous forces provide a perturbation, that is still a challenge. As flow rate decreases, computational time increases and direct simulation on larger images becomes difficult. The most known method is lattice Boltzmann (Blunt et al., 2013).

An alternative to DNS is pore network modeling (PNM), a widely used and long-established approach for transport simulations in porous materials. The original motivation for PNM development was to study the effect of multiphase conditions on transport in porous materials. Major advantage is simulation over millions of pores and throats in respect to hundreds feasible by DNS. Pore network modeling facilitates multiphase flow (Gostick, 2017). In principle, pores are defined as larger voids in the pore space, and throats are smaller pathways that are connecting the pores. There is always the question of whether something is a pore or a throat. After the network is extracted, pores and throats are assigned properties such as volume, shape and inscribed radius. Various algorithms are used to determine which pores belong to which throats, and how the entire network is connected. One of the most used methods in paid software is Maximum ball. Spheres are grown in the pore space, centered in each void voxel; the largest represent pores, while chains of smaller spheres are defined as throats (Figure 2-3.). This method is effective for larger pores, but tends to create smaller elements until image resolution is reached (Blunt et al., 2013).
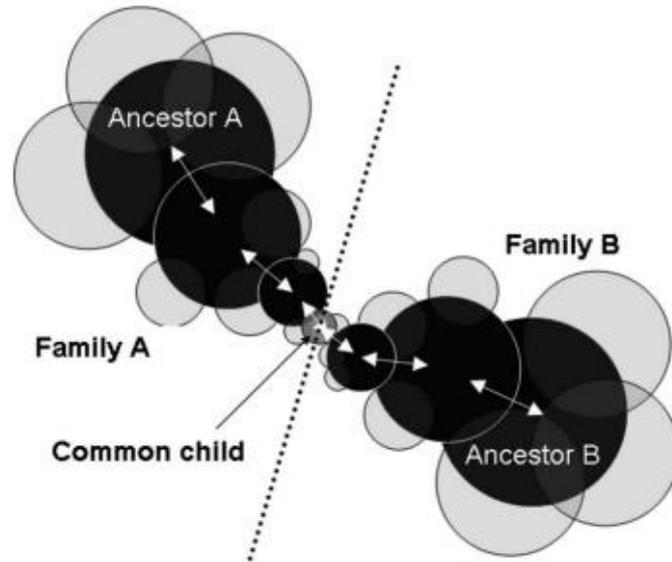
Figure 2-3. Schematic of two families A and B, the ancestors, their common child defining the throat and the pore-throat chains along white arrows (Dong & Blunt, 2009)

In their paper, Rabbani et al. (2014) revisited a new computational algorithm for pore network extraction, known as *watershed algorithm*, proposed by Thompson et al. (2008) and Sheppard et al. (2006). In this method, pores and throats are detected and separated using distance function and watershed segmentation. The basic idea is to use a binary image that contains 1 for grains or solids (black) and 0 for pores or voids (white), as a topographic surface. Since each pixel has a depth, the algorithm identifies local minimums, and treats them as *Catchment basins* that are starting points of a flood. When two basins reach a contact line, called watershed ridge line, they become segmented regions – detected as pores and separated with a throat. For better understanding, see Figure 2-4., where two binary objects are connected (Rabbani et al., 2014).
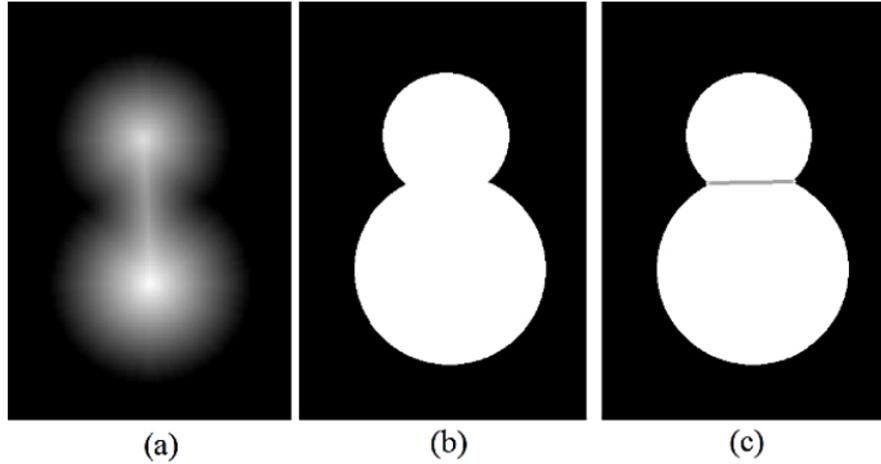
Figure 2-4. (a) Grayscale distance map. (b) Original binary image. (c) Segmented pores (Rabbani et al., 2014)

To obtain a distance map, Euclidean distance is calculated:

$$D_b = \sqrt{(x_b - x_i)^2 + (y_b - y_i)^2} \tag{2-1}$$

where D_b is distance between a specific white pixel (x_i, y_i) and an arbitrary black pixel (x_b, y_b) (Rabbani et al., 2014).

The process of pore network modelling is performed using SNOW (Subnetwork of the Oversegmented Watershed, Gostick, 2017) algorithm, previously coded and written into the PoreSpy module. Together with OpenPNM, these modules contain the source code for the SNOW algorithm (Sušilović, 2020). OpenPNM is a package for performing pore network simulations of transport in porous materials containing 10 modules (OpenPNM, 2023). PoreSpy is a collection of image analysis tools used to extract information from 3D images of porous materials (typically obtained from X-ray tomography) containing 8 modules (PoreSpy, 2023).

In 2020, to obtain an extracted pore network, several steps were performed:

    1. reducing the number of peaks by filtering the distance transform with a Gaussian blur

    2. removing peaks that actually fell on plateaus and saddles in the distance transform

    3. removing peaks that were too near another peak (Gostick, 2017).

In 2023, *PoreSpy documentation* published that *snow2* function was created to combine these steps into a single function for simplicity. To visualize the extracted pore network, *Paraview* software is used. *Stick and ball* model can be seen in Figure 2-5.
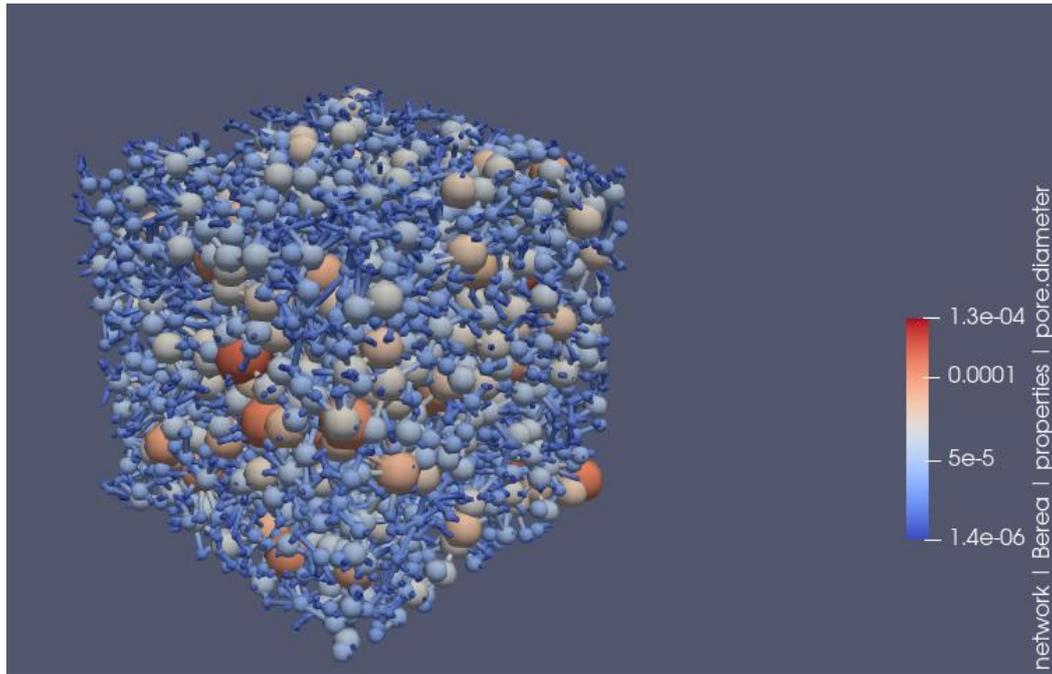
Figure 2-5. Stick and ball model of a Berea sandstone (Sušilović, 2020)

2.3. Upscaling methods

Multiphase flow in porous media is manifested at various scales and physical description on one scale can be used to obtain and analyze the same properties at a higher scale. It is important to understand multiphase flow and reactive transport processes at microscopic scale and upscale it to the macroscopic scale (core or field scale). It is mostly done by averaging, but as a result, processes at local-equilibrium may require a non-equilibrium description on a field scale. Often in studies, core medium is considered highly heterogenous, and when upscaled, homogeneous description is concluded. Multiphase flow behavior on a macro scale is based on an empirical extension of a Darcy's law together with Pc-Sw-kr relationships (Hassanizadeh et al., 2005).

Valvatne et al. *(*2005) show how the flow properties for Berea can been estimated using pore scale modeling with a topologically disordered lattice of pores connected by throats. Distribution of pore sizes can be tuned to match capillary pressure data. To capture a static pore network, 3D voxel representation of the rock needs to be reconstructed. Using microtomography the rock can be imaged with a resolution of microns (Dunsmuir *et al*., 1991; Spanne *et al*., 1994.). From this voxel representation an equivalent network containing pore and throat volumes, diameters, etc can then be extracted (Øren and Bakke, 2002).

For predicting multiphase fluid flow, effects of heterogeneity have to be recognized and analyzed at a variety of length-scales. Sometimes, multistage upscaling is present, from small scales (mm or cm) to full-field scale (m or km). Heterogeneity is not contained only in permeability and rock types, but in interaction of fluid forces on different scales (capillary, viscous and gravity) (Pickup et al., 2005). Pickup et al., studied two approaches of upscaling:

Steady-state method. When two phases are present, relative and absolute permeability are upscaled. The simplest method assumes that the fluids are in steady state (SS), meaning saturation does not change over time, $\frac{\partial S_w}{\partial t} = 0$. Both, capillary equilibrium and viscous-dominated SS can be upscaled using this method. For the viscous flood, fractional flow is considered constant along streamlines. Also, when the flood is gravity-dominated, the fluids reach an equilibrium (Pickup et al., 2005).

Two-phase dynamic. Two-phase flow simulation is required on a local fine grid. It is extremely time (processor) consuming and the results obtained may not be as reliable (Barker and Thibeau, 1997). Advantage is that the upscaled relative permeabilities can compensate for the increase in numerical dispersion as the grid is coarsened. To reproduce the water distribution for the correct force balance, a fine-scale two-phase flow simulation is used. The dispersion of the front due to heterogeneities in permeability is taken into account. The average pressure of the individual phase is computed (Pickup et al., 2005).

3. INPUT DATA AND ANALYSIS PROCEDURES

Upscaling workflow for this study includes choosing representative geological, petrophysical, fluid and reservoir data as well as experimental and digital methods such as simulation code, laboratory measurements and software (Table 3-1.). Typical workflow is presented in the Figure 3-1.
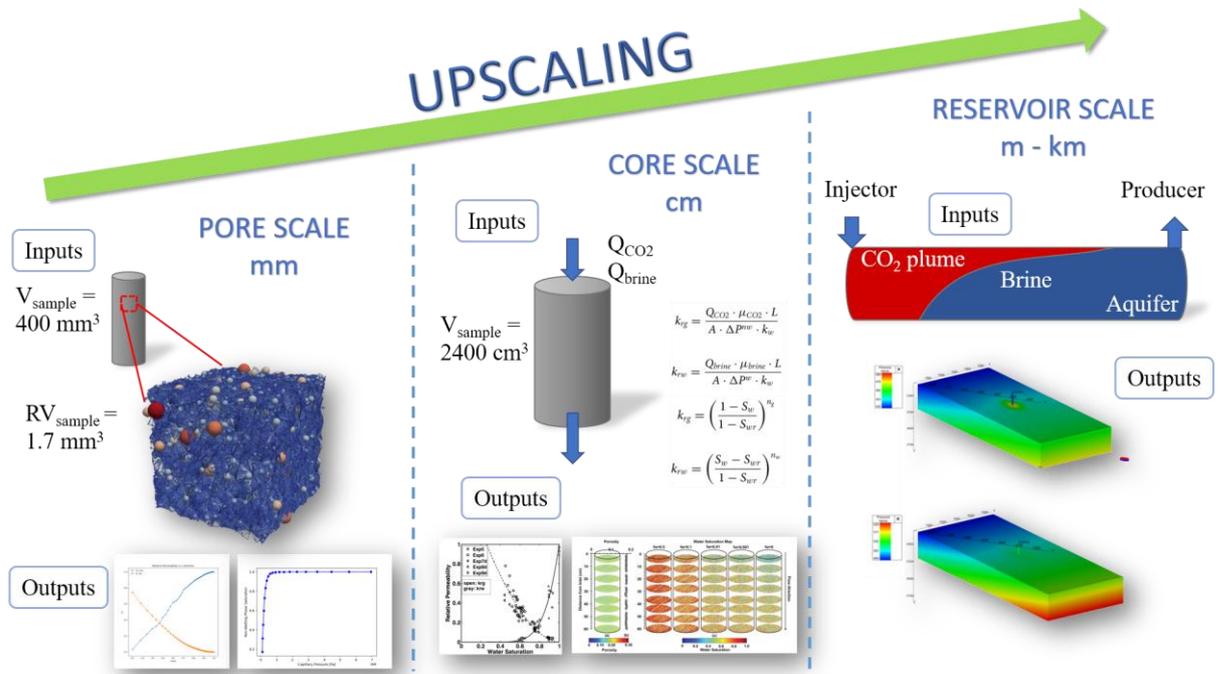
Figure 3-1. Upscaling workflow used in this study.

Table 3-1. Overview of important parameters regarding each scale.

	PORE SCALE	CORE SCALE	FIELD SCALE
Rock & Fluids	• Berea sandstone • CO_2 and water	• Berea sandstone • CO_2 - brine	• Sava-East regional aquifer • CO_2
Experimental & digital methods	• Core drilling • Micro CT scanning • Image processing • Simulation code	• Steady state primary drainage • Medical CT scanning	• Reservoir simulation of CO_2 injection into a deep saline aquifer
Software & packages	• 3D reconstruction software • ImageJ • Python modules OpenPNM and PoreSpy • Excel, Paraview	• tNavigator (Coreflood numerical simulation)	• tNavigator

3.1. Pore scale

Most-referenced rock type is Berea sandstone, which can be considered as a representative rock for Croatian sandstones. Moreover, Berea was selected for this study to facilitate the comparison between results. It is a finer-grained, well-sorted sandstone with closely spaced planar bedding (Churcher et al., 1991).

Core description and preparation. Core preparation includes drilling a regular sized core with a drill bit (OD=8 mm and ID=5.5 mm) to achieve the proper size for the scanning (Figure 3-2.). The drilled cylindrical core sample had 2 cm in length and 5 mm in diameter (Figure 3-3.). It was mentioned earlier that the size of the core is one of key parameters in preserving high resolution of a microCT scan. Meaning, the size must be in millimetres rather than micrometres to achieve a resolution of one micrometre.

Figure 3-2. Drilled core sample (Left). The drill bit (Right).

Figure 3-3. Drilled Berea sandstone sample.

Further, the sample for the scan was prepared. Dental wax was used to attach a sample to the object holder of a microCT scan. Object holder together with the glued sample was fixed in the holder's casing (Figure 3-4.). Scanning process was initiated.
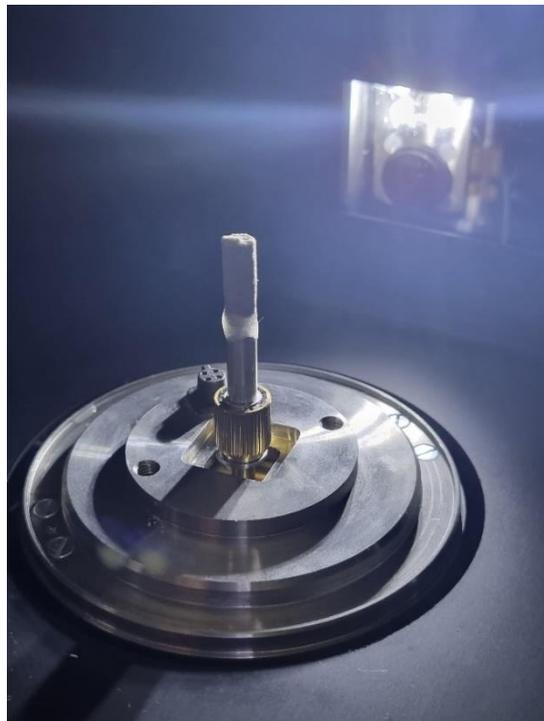
Figure 3-4. Berea sample fixed inside the microCT object holder.

Scanning and image processing. The core was scanned with Bruker's high-resolution 3D X-ray microCT scan, model SKYSCAN 1272 CMOS edition (Figure 3-5.).
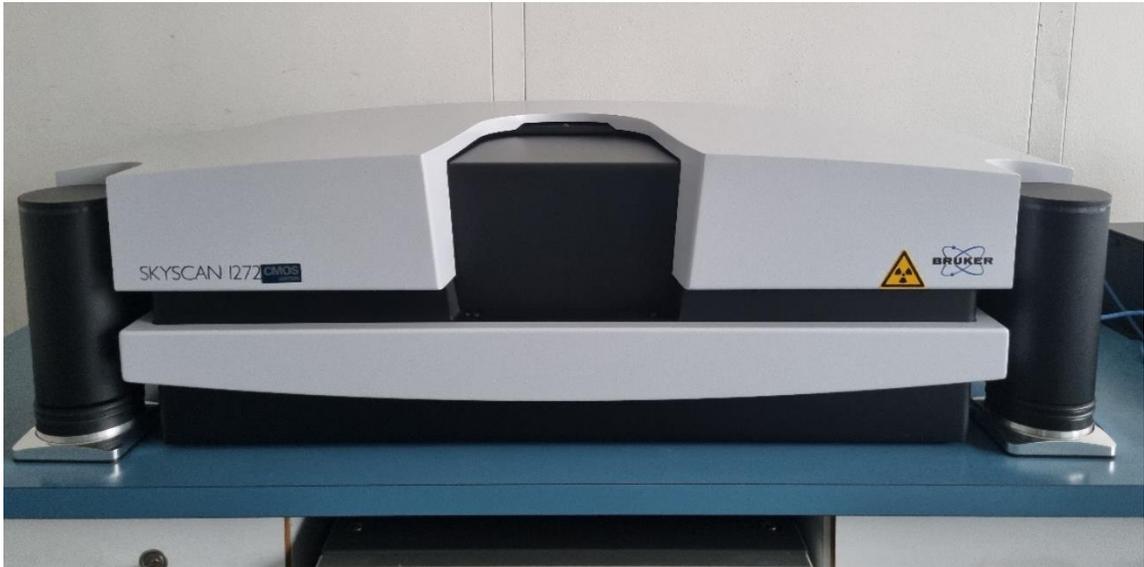
Figure 3-5. Bruker's microCT scan, model SKYSCAN 1272 CMOS edition.

Before scanning, the machine had to be calibrated to work properly. Optimal scanning parameters that were mostly used for this process are an X-ray source voltage of 80-90 kV and a power of 4-6 W.

The scanning of the core lasted 15 hours, and during this time the device tdid not need to be observed or stand next to it. Even though the X-ray beam source is extremely secured with lead meaning that the radiation circle decreases with distance (the range is about 20 centimeters), it would actually be safer to leave the room. Usually, the sample rotates at micro CT stage 360° with an increment of 0.1°-0.2° resulting in approximately 1800-3600 projections (3-1).

$$\frac{\text{Camera stage mode}_{\,360° \text{ or } 180°}}{\text{Projection increment}} = N_{projections} \qquad (3\text{-}1)$$

In this case, computer software produced 1800 2D projections (images) of 1.5 μm pixel size (resolution) and 4096 pixels. This means that only 6 mm of a 2 cm long core is visible and the rest is outside the field of view (3-2).

$$L_{\text{scanned object}} = N_{pixels} \cdot \text{resolution} \qquad (3\text{-}2)$$

Accordingly, the width of the scan is 6 mm, and our sample is 5 mm wide, leaving 0.5 mm on each side for air (Figure 3-6.). When there is not enough air space surrounding the sample, S/N is lower, therefore noise is higher, and image quality is lower.
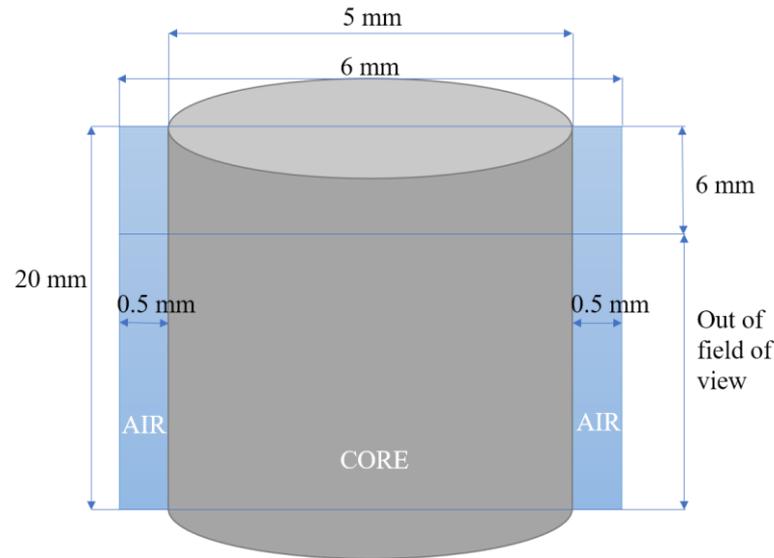
Figure 3-6. Sketch of a scanned core (gray), 2D projection (blue) and air surrounding it.

Prior to reconstruction, image processing is done by means of applying various filters. The aim is to remove all artefacts observed as rings which appeared during the scanning and increase the overall image quality in terms of details. Additionally, heterogenous materials are created due to beam hardening effect. The next step is volume rendering where reconstructed results are displayed as a realistic 3D object starting with transparency, opacity, brightness and contrast adjustments. Since the 3D model is too large and computationally demanding, the original volume is cropped into an 800^3 subvolume (Figure 3-7.). Further, we start image processing in ImageJ to obtain binary images. Thresholding is adjusting the porosity in the slicer and promptly observing the histogram by increasing the pore space volume. This interpretation is subjective and can vary substantially, resulting in different petrophysical properties. The porosity of our Berea sample of 17.19% was calculated from an image in ImageJ. The software converts this 800 slice stack to binary values and produces 8-bit images with 0 and 255 values (black and white). The image is saved in .tif format. Figure 3-8. shows one slice of processed image.
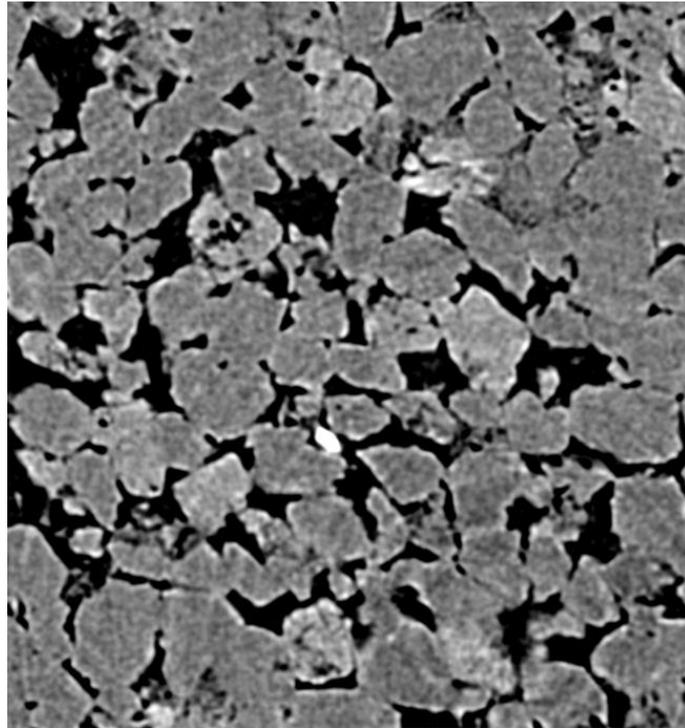
Figure 3-7. First slice of unprocessed image.
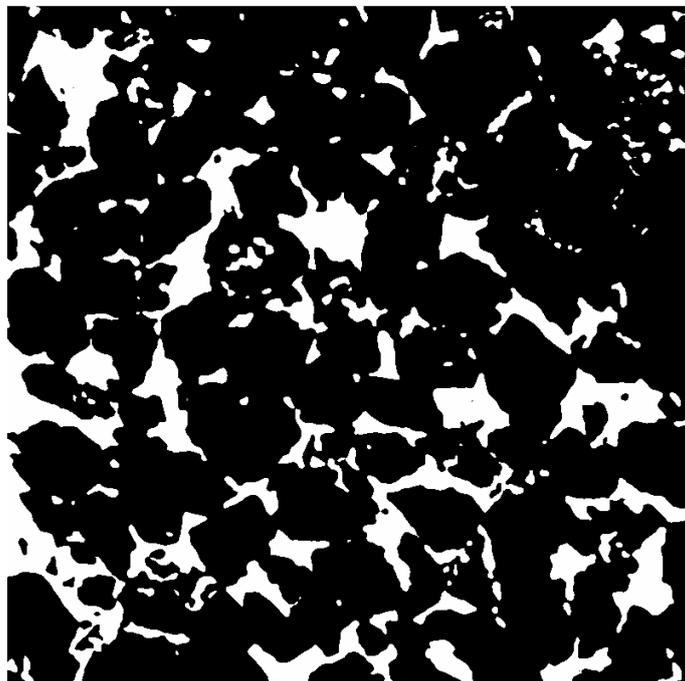
Figure 3-8. First slice of processed image.

Simulation code. The relative permeability curve is obtained using code written in the Python programming language. Full code can be found in the Appendix 1. A simulation takes 40 minutes to generate results.

It starts by importing OpenPNM and PoreSpy open source packages. A previously processed binary image (zeros and ones) in .tif format is imported and Python reads the data as Boolean type data (true or false).

Pore network is extracted using the *snow2* algorithm, which can perform multiphase extractions. We defined the image as a *phase* and used *phase_alias* to assign a desired value of phase to each voxel with– „void" as „true" and „solid" as „false" values. In addition, the voxel size of 1.5 µm must be specified. The next step is giving the PNM skeleton some structure by adding geometry of spheres and cylinders, which can also be visualized in Paraview. Defining the boundaries of the model is important in order to perform various simulations. PNM is an object that contains coordinates where minimum and maximum coordinates as „left" and „right" markers are defined. The Topotools module finds the pores on the surface of the domain by performing a Delaunay triangulation between the network pores and our defined markers. All pores connected to these marker points are considered as surface pores (OpenPNM, 2023).

Prior to flow simulation, we create phases by assigning fluid properties of water and air such as viscosity, density, interfacial tension and contact angle. These input parameters are crucial for alternating relative permeability curves. Table 3-2. shows four examples of input data for simulation.

Table 3-2. Four examples of input data for simulation. Values coloured red present parameters used to alternate kr curve.

Parameter [Unit]	Example 1		Example 2		Example 3		Example 4	
	CO_2	Water	CO_2	Water	CO_2	Water	CO_2	Water
IFT [N/m]	0.035	0.035	0.035	0.035	0.035	0.035	0.035	0.035
Contact angle [°]	20	160	30	150	20	160	20	160
Density [kg/m^3]	850	1000	850	1000	900	1000	800	1000
Viscosity [Pa*s]	8.87E-05	0.001	8.87E-05	0.001	8.87E-05	0.001	8.87E-05	0.001

Contact angle and interfacial tension were obtained from scientific articles. A study on CO_2-brine contact angles on various rock proved experimentally that the sCO_2 contact angle at the temperature of 45°C for Berea, ranges between 15 and 27° (Table 3-3.). Therefore, angles 30° and 20° for CO_2; 150° and 160° for water were chosen. Interfacial tension between CO_2 and water is shown in Figure 3-9. It was measured as a function of pressure. In addition, data compiled from the literature also given. Interfacial tension decreases as CO_2 pressure increases, and it remains constant once it reaches the critical CO_2pressure of about 73 bars (CO_2 vapour-

liquid boundary). Values for density and viscosity were taken from the *NIST (National Institute of Standards and Technology) Chemistry WebBook* (2021).

Table 3-3. Variation of contact angles due to local surface roughness (Haeri, 2020).

Rock type	Bubble diameter (µm)	Contact angle (°) Sc-CO$_2$ (1800 psi, 45°C)	Contact line (µm)
Berea	835 (±15)	27 17	285 240
	1445 (±25)	24 15	605 510

Figure 3-1. Interfacial tension between water and CO$_2$ (Espinoza et al., 2010)

Invasion Percolation (IP) is a volume-controlled injection in which a specific incremental volume amount is injected that corresponds to the volume required to invade the next available throat or pore. The actual pressure applied varies depending on the size of the neck being invaded. The IP algorithm is implemented from the left surface pores in the x direction. As a result, invasion sequence is obtained, which contains the entire invasion history in a single array. Saturation of the fluid at a certain point in pores and throats is then found by

occupancy occupying of the phase, using invasion sequence and some calculations directly. In the custom function, pore mask and throat mask arrays were determined, which are exactly a limit of invasion sequence at that point. The sum of the volumes at this point represents saturation of pores (3-3) and throats (3-4) at the limit. Dividing this sum by bulk volume (3-5), gives a saturation point (3-6) (OpenPNM, 2023).

$$S_{pore} = \sum V_{pore@pore\ mask} \tag{3-3}$$

$$S_{throat} = \sum V_{throat@throat\ mask} \tag{3-4}$$

$$V_{bulk} = \sum V_{pore} + \sum V_{throat} \tag{3-5}$$

$$S = \frac{S_{pore} + S_{throat}}{V_{bulk}} \tag{3-6}$$

Relative permeability is the ratio of effective to absolute permeability. If the boundary condition and viscosity are the same, geometry will cancel out leaving the ratio of flow rates (3-7).

$$K_{rphase} = \frac{K_{ephase}}{K_{abs}} = \frac{Q_{e-phase}}{Q_{abs-phase}} \tag{3-7}$$

To determine absolute flow rates, Stokes Flow algorithm with hydraulic conductance model was applied. This means that a model is assigned for a single-phase flow. The assignment of multiphase conductance models to the phases takes into acccont the presence of the other phase in effective permeability. Since the focus is on relative permeabilities in x direction, inlet and outlet flow as left and right pores were defined. After defining necessary models and functions, for each example a set of relative permeabilities for CO_2 and water over a range of 100 saturations for more qualitative approximation of the kr curve were obtained.

One of the main applications of the *Drainage* algorithm is the simulation of capillary pressure curves, specifically Mercury Intrusion Porosimetry. The inlet capillary pressures were calculated using the Young-Laplace equation (3-8) assuming that the throat is a cylindrical tube. Trapping does not occur in an MIP simulation since the wetting phase (air) is evacuated prior to mercury injection, Nevertheless, trapping can be applied and the effect is that the non-wetting phase does not reach the saturation of 1 (OpenPNM, 2023).

$$P_c = - \frac{2\sigma(\cos(\theta))}{r} \tag{3-8}$$

      Absolute permeability was calculated using Stokes Flow algorithm with constant pressure boundary conditions in x direction. Algorithm returns the cumulative flow rate of a phase. Simply, Darcy's law was used to calculate K_{abs}:

$$K_{abs} = \frac{Q \mu L}{A \Delta P} \tag{3-9}$$

where Q is the inlet flow rate, A is the area of a sample (3-10), and L is the distance between inlet and the outlet (3-11).

$$A_{sample} = (N_{voxel} \cdot resolution)^2 \tag{3-10}$$

$$L_{sample} = N_{voxel} \cdot resolution \tag{3-11}$$

3.2. Core scale

Core scale includes a coreflood experiment, obtained form an article, and a coreflood numerical simulation, to compare both datasets with the pore scale. Additionally, it will be used for further upscaling.

3.2.1. Coreflood laboratory experiment

Considering several months of extensive laboratory measurements of steady-state relative permeabilities (a part of special core analysis, *SCAL*), and the expensive equipment required for these experiments, analysis on a core plug was obtained from an article published in 2016 in an online-only scientific journal *Greenhouse Gases: Science and Technology*. Chen et al. (2016) performed *steady state* laboratory analysis, also using core plug Berea sandstone, in which both non-wetting (CO_2) and wetting (brine) fluids are injected simultaneously, and at the same rate, until a stable fractional flow is established, allowing direct determination of relative permeability.

Materials. Measurement of CO_2-brine relative permeability was done by performing five steady-state primary drainage experiments in a 116 mD Berea sandstone core plug at 20°C and 10.34 MPa using pressure taps. The core plug was 60.8 cm long and 7.14 cm in diameter. At mentioned p-T conditions brine (2%wt NaCl) and CO_2 concurrently flowing in the core as two liquid phases. The viscosities of the equilibrated CO_2 and brine are 0.000087 Pa*s and 0.001081 Pa*s, respectively. The density of the non-equilibrated is 1011.7 kg/m^3 and 860.4 kg/m^3 for non-equilibrated CO_2.

Coreflood experiment. The rock sample was wrapped with three layers in order to provide barriers for injected brine and CO_2. It was placed in a Vitton rubber sleeve inside a vertically placed aluminium core holder. Water was pumped between the rubber sleeve and the core holder to confine pressure of 13.8 MPa. From the inlet to the outlet, four pressure taps were drilled through the core at certain positions creating five sections where pressure drop was continuously monitored using pressure transducers. Two dual-pump systems were used to inject brine and CO_2 from two accumulators. Figure 3-10. shows the experiment scheme.
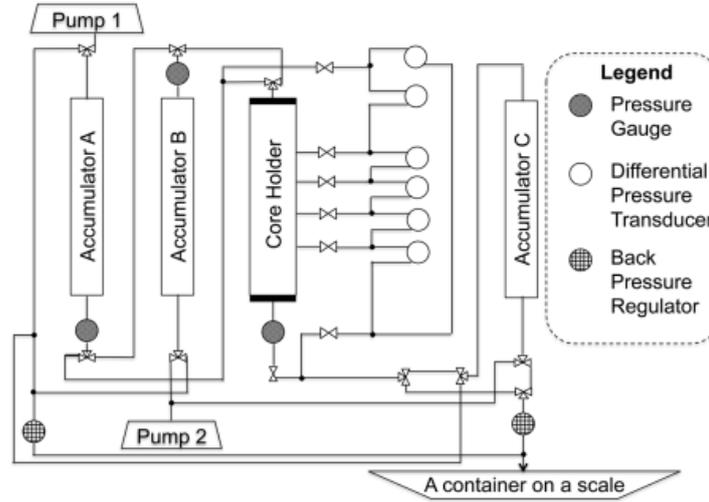
Figure 3-9. Schematic set-up of core flooding apparatus (Chen et al., 2016).

Porosity and saturation were determined using a medical X-ray CT scanner and the voltage of 140 kV. The core holder was placed onto a vertical positioning system that allowed it to move up and down the scanner. Total of 52 one-cm slices of CT scans were shot. Linearity between the CT number and density is contained in two equations which were used to calculate porosity and saturation.

$$\Phi = \frac{CT_{wet} - CT_{dry}}{CT_{brine} - CT_{air}} \qquad (3\text{-}12)$$

$$S_w = \frac{CT_x - CT_{CO2sat}}{CT_{brinesat} - CT_{CO2sat}} \qquad (3\text{-}13)$$

where CT_{brine} and CT_{air} are the CT numbers of non-equilibrated brine and air, 14 and -1000, respectively.

The first step of the experiment is displacing non-equilibrated brine with equilibrated one. In the second step, equilibrated brine and equilibrated CO_2 were co-injected at specified flow rates until steady-state is reached. Indication of the steady-state is overall pressure drop and the stable pressure drop of five sections of the core and the saturation profile along the core did not change with time. Flow rates were alternated with a lower water fractional flow (f_w). Experiment was run to 100% CO_2 injection. Finally, five primary drainage experiments were done, three of which included five steps and two of which only had 100% CO_2 injection, as shown in Table 3-4. (Chen et al., 2016).

Capillary desaturation curve is an empirical relationship between the residual phase saturation and the capillary number (Figure 3-11.). Capillary number is a dimensionless number which quantifies the ratio of viscous to capillary forces. Generally, it is defined as:

$$Ca = \frac{F_{viscous}}{F_{capillary}} = \frac{\mu\upsilon}{\sigma} \tag{3-14}$$

where υ is the interstitial velocity and μ the pore scale viscosity of the displacing fluid. The force opposing viscous regime is the interfacial tension (Guo et al., 2022.). All five experiments are within capillary dominated flow because the capillary number is less than 10^{-6} (Chen et al., 2016).

Finally, using two phase Darcy's law relative permeability values were calculated (3-15) (3-16). Corey type models (3-17) (3-18) were also calculated that fit to the kr curves using a least square method.

$$k_{rg} = \frac{Q_{CO2} \cdot \mu_{CO2} \cdot L}{A \cdot \Delta P^{nw} \cdot k_w} \tag{3-15}$$

$$k_{rw} = \frac{Q_{brine} \cdot \mu_{brine} \cdot L}{A \cdot \Delta P^{w} \cdot k_w} \tag{3-16}$$

$$k_{rg} = \left(\frac{1-S_w}{1-S_{wr}}\right)^{n_g} \tag{3-17}$$

$$k_{rw} = \left(\frac{S_w-S_{wr}}{1-S_{wr}}\right)^{n_w} \tag{3-18}$$
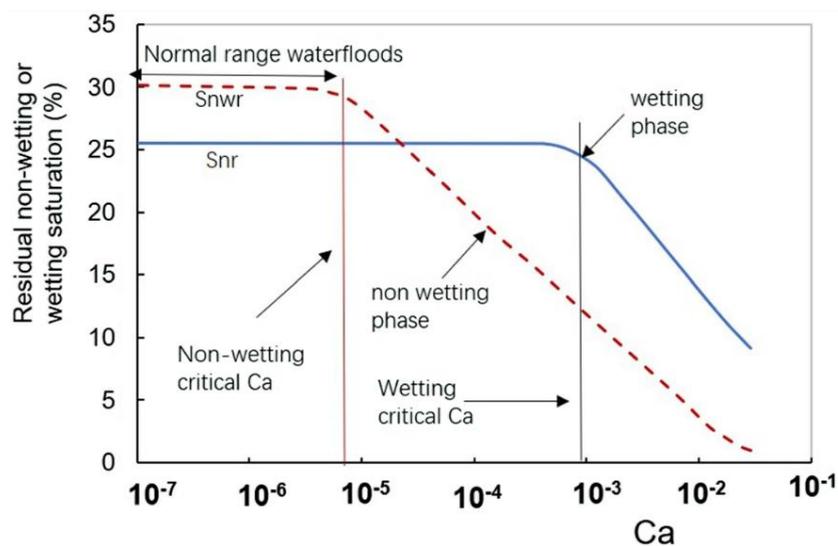

Figure 3-10. Capillary desaturation curve (Guo et al., 2022).

Table 3-4. Injection rates during each primary drainage experiment (Chen et al., 2016)

	Qbrine:QCO$_2$	100:0	50:50	10:90	1:99	0.1:99.9	0:100
Exp5	Qbrine(ml/min)	2.000	1.000	0.200	0.040	0.008	0
	QCO$_2$(ml/min)	0	1.000	1.800	3.960	7.992	8.000
Exp6	Qbrine(ml/min)	4.000	2.000	0.400	0.080	0.016	0
	QCO$_2$(ml/min)	0	2.000	3.600	7.920	15.984	16.000
Exp7d	Qbrine(ml/min)	2.000	1.000	0.200	0.020	0.002	0
	QCO$_2$(ml/min)	0	1.000	1.800	1.980	1.998	2.000
Exp8d	Qbrine(ml/min)			NA			0
	QCO$_2$(ml/min)						2.000
Exp9d	Qbrine(ml/min)			NA			0
	QCO$_2$(ml/min)						4.000

3.2.2. Coreflood numerical simulation

The following phase in the study is a comparison and effort to reconcile the so-called pore-scale model (modeled at the pore level using CT-scan) and core-scale model (laboratory experiment of CO$_2$ injection into the core). In this scenario, an input file was created based on data from the literature (Chen et al., 2016), and it was ran with the computer software tNavigator (Rock Flow Dynamics, RFDyn, 2022).

In particular, the injection of CO$_2$ and water in the laboratory causes corrosion and severe damage to expensive equipment. As a result, such measurement data is valuable and extremely rare. Simulation of a core plug flooded by a fluid has been modeled previously, usually as a 1D model (number of cells in j and k direction NY = NZ = 1), and as an *unsteady state* displacement experiment (the core is initially saturated with one fluid up to critical saturation of the wetting fluid, usually brine, and then another fluid, such as water, water-polymer solution, CO2 or other gases are injected as displacement fluids).

Because a 3D coreflood model with flow through cylinder was created (Figure 3-12.), Python code was written to quickly test various gridblock sizes (Figure 3-13.). The cylinder geometry was created using a block-centered grid and setting ACTNUM parameters, to determine which cells are active and which are inactive. The model dimensions are NX×NY×NZ = 26×31×31, with cell dimensions DX = 2.3385, DY = 0.2303, and DZ = 0.2303 (cm), for a total of 24986 cells. At (x, y) = 1, 16 are placed both CO$_2$ and brine injection "wells" (coreflood inlet), and at 26, 16 is placed production "well" (coreflood outlet). All wells have a diameter (d_w) of 0.2 cm and are set to inject at constant reservoir volume rate (control mode =

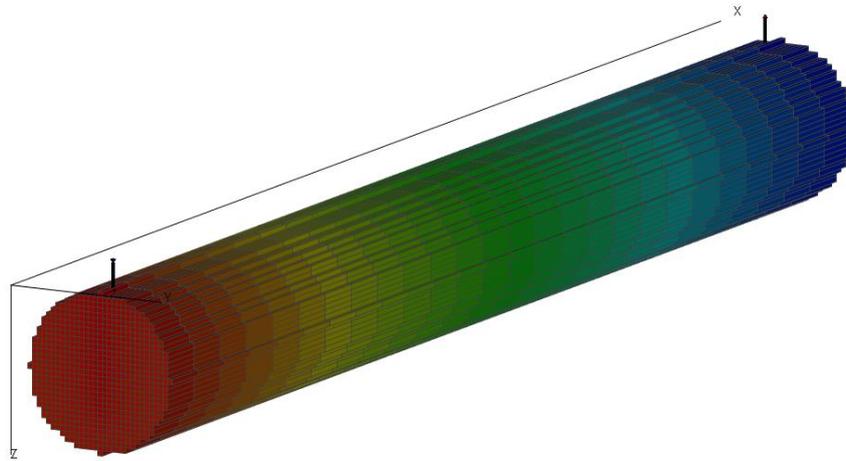RESV). The RESV at the outlet is equal to the sum of the both RESV parameters (CO2 and brine) at the inlet.

Figure 3-11. Cylindrical geometry for coreflood model in tNavigator.

```python
1 # -*- coding: utf-8 -*-
2 """
3 @author: domagoj
4 """
5
6 import numpy as np
7
8 def mesh_circle(diameter, ny, nz):
9     radius = diameter * 0.5
10    # create a meshgrid
11    y = np.linspace(-radius, radius, ny)
12    z = np.linspace(-radius, radius, nz)
13    y, z = np.meshgrid(y, z)
14
15    # distance of each element from the center of the circle
16    dr = np.sqrt(y**2 + z**2)
17
18    # True values are at cells inside the circle
19    mask = dr <= radius
20
21    return (mask*1)
22
23 #coreflood number of cells
24 NX, NY, NZ = 26, 31, 31
25 diameter = 7.14
26 length = 60.8
27 #coreflood dimensions of cells
28 DX, DY, DZ = length/NX, diameter/NY, diameter/NZ
29 circle = mesh_circle(diameter, NY, NZ)
30 gridblocks = np.array([circle]*NX)
31 a = gridblocks.flatten(order = 'F')
32 np.savetxt('ACTNUM.inc', a, fmt='%s', header = 'ACTNUM', footer = '/',
33 comments='')
```

Figure 3-12. Computer code to form a circle intersection in the X-direction for ACTNUM parameters.

3.3. Reservoir scale

The following characteristics are assumed for CO_2 aquifer storage for a reservoir scale simulation (data similar to a region in the Sava-East regional aquifer, Vangkilde-Pedersen et al., 2009, Figure 3-14.): minimum cap rock depth = 2330 m, maximum cap rock depth = 2575 m, constant effective height of a formation is H_{ef} = 150 m, permeability in x and y direction k_x = k_y = 17 mD and porosity $\phi = 0.18$.
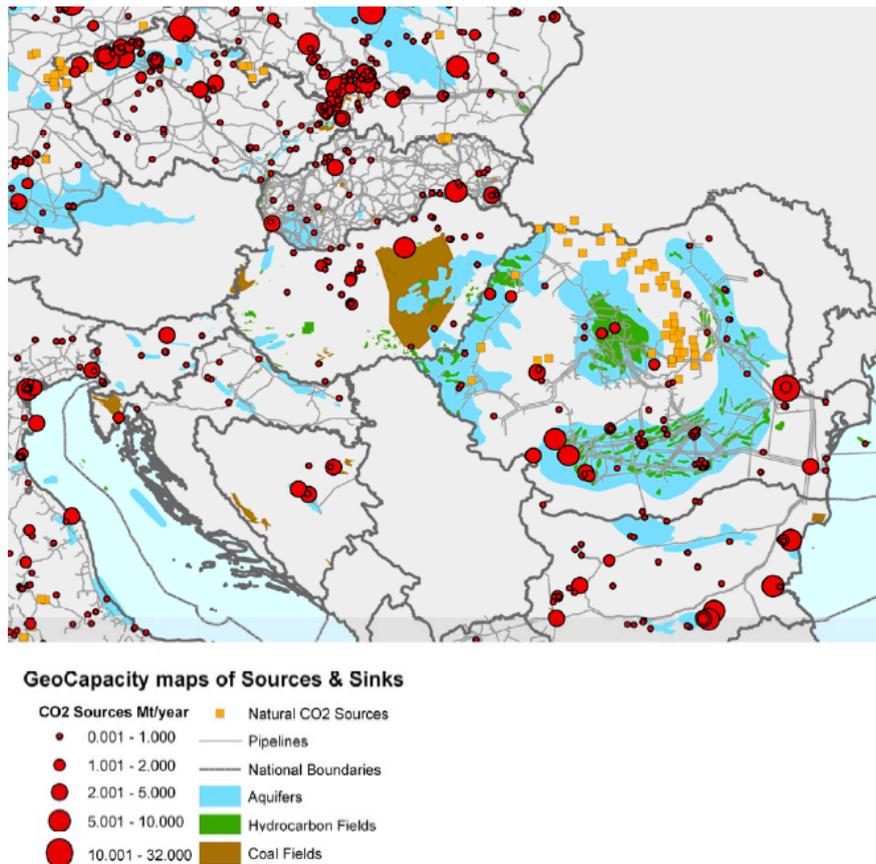
Figure 3-13. Figure derived from the first Pan-European comprehensive CO_2 storage potential mapping (Vangkilde-Pedersen et al., 2009, Project).

To see how different saturation tables (defined in tNavigator with SWFN and SGFN keywords) affect the CO_2 injection process, with emphasis on pressure and CO_2 plume migration, simulation input file template was used. The template was modified to exclude all uncertain factors that concern fluid properties and rock properties, so the CO2STORE option was used.

Many CO_2 storage simulation studies have been performed at the Faculty of Mining, Geology, and Petroleum Engineering (University of Zagreb). After initial screening, mapping,

and data collection for FP EU GeoCapacity (Vangkilde-Pedersen et al., 2009) and CO2Stop (Poulsen et al., 2015) projects, models have been developed for both, onshore and offshore sites, and various simulation studies have been published (such as Vulin et al., 2018; Saftić et al., 2019; Vulin et al., 2020; Arnaut et al., 2021; Jukić et al., 2022). However, the CO2STOR option was avoided in the simulator, because of oversimplification (correlation) of PVT fluid properties. Nevertheless, it seems reasonable to use this option in this work to isolate the transport parameters (permeability, relative permeability) in the system. Only CO_2 and water were employed, and salinity was not considered. The compressibility of the rock was assumed to be $c_f = 10^{-5} bar^{-1}$.

The model was equilibrated and initialized at datum depth $h_{ref} = 2445\,m$, with a small underpressure (p=240 bar) assumed. Other factors, such as water-oil contact or gas-oil contact, have no effect on the simulation model's setup but can reduce the number of warnings.

A good assumption (according to the data in the nearby oil reservoirs) is that the temperature is around 150°C, but in detailed studies, temperature changes of CO_2-brine solubility (and CO_2 density) should be considered. For simplicity, a single well was used, and since some parts of formation are naturally fractured, it was assumed that 1E6 sm3/day of CO_2 could be injected. This amount is equal to a dynamic capacity of about 0.683 Mtpa, and since the injection was simulated over 20 years period, this results with storage capacity of around 13,5 Mt. After the well was closed, simulation was continued over a period of 55 years, to the year 2100, to observe plume migration and pressure distribution.

4. RESULTS

The results were obtained from previously mentioned pore network modelling on a pore scale, coreflooding experiment and numerical simulation on a core scale, and the simulation of CO2 injection in to a deep saline aquifer on a reservoir scale.

4.1.   Pore scale

Results obtained from the multiphase flow simulation, are visualized in Excel. All four sets of relative permeabilities and their associated curves show more or less similar data values and shapes of the curve. Wetting phase relative permeabilities (kr_w) show little to no variation, while non-wetting phase relative permeabilities (kr_{nw}) differentiate mostly when the contact angle between water and CO_2 is changed, from 160° to 150° and 20° to 30°, respectively (see Examples 1 and 2 in Table 3-2.). Increasing the CO_2 density, lowers the curve exponent, indicating slower CO_2 flow in a two phase system (Example 3). Interestingly, CO_2 density of 800 kg/m3 (Example 3) shows lower kr values than the density of 850 which is the optimal value of the CO_2 density (Example 1). Since, the trapping of the phases is neglected and no parameter such as critical water saturation was determined in the simulation, both phases are immediately mobile. Consequently, there is no capillary end effect. Including a threshold, where kr_{nw}/kr_w=1E-4, it can be seen that CO_2 begins to displace the water at a critical saturation, S_{gc} = 0.92. Water mobility extremely decreases when S_w=0.8 is reached, after which the exponent decreases. A higher CO_2 mobility is gained at 0.77. After saturation point between 0.67 and 0.68 has been reached, CO_2 has greater mobility and displaces the water (Figure 4-1.)

Capillary pressure curves were calculated only for Examples 1 and 2 because the main modification parameter was contact angle. The result are two very similar curves when capillary trapping is applied (Figure 4-2.). They both reach a plateau at S_{wnp}=0.9 with a maximum pressure of about 0.3 MPa. Meaning, 0.1 of the residual saturation of the wetting phase, which is in this case air.

Calculated absolute permeability is 125 mD which is in the range of the Berea core scale (116 mD).
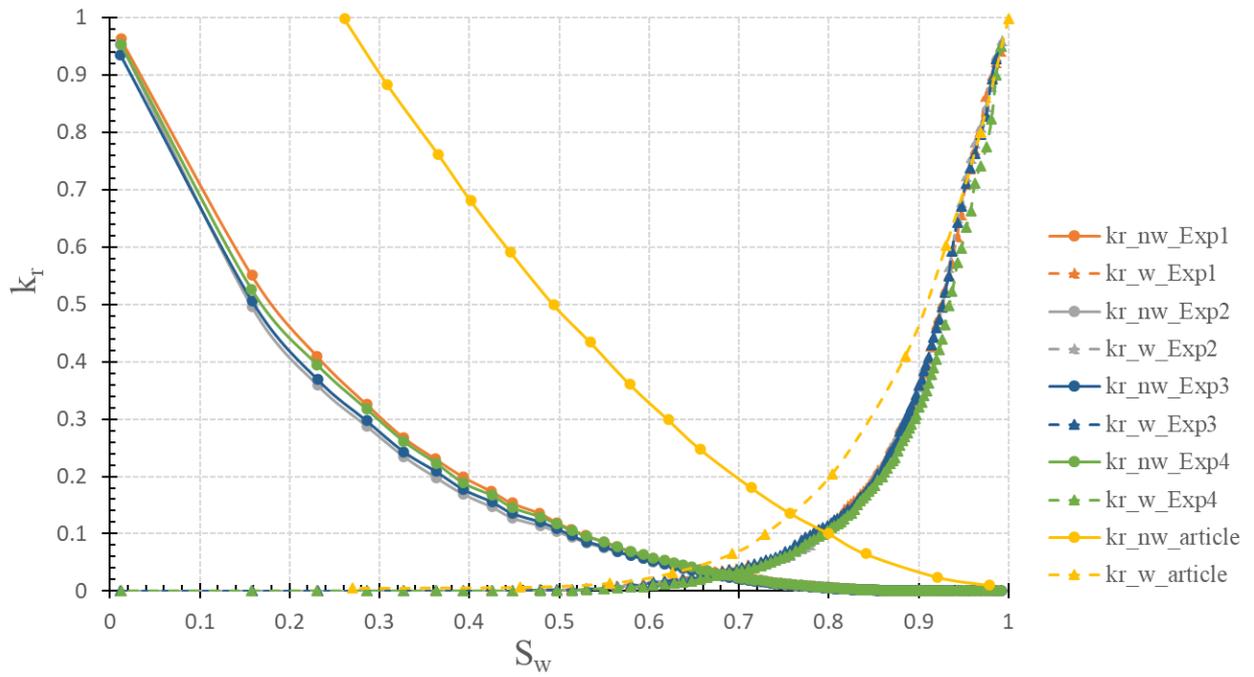
Figure 4-1. Relative permeability curves for wetting phase (water) and non-wetting (CO_2) phase. Legend contains marks for associated experiments.
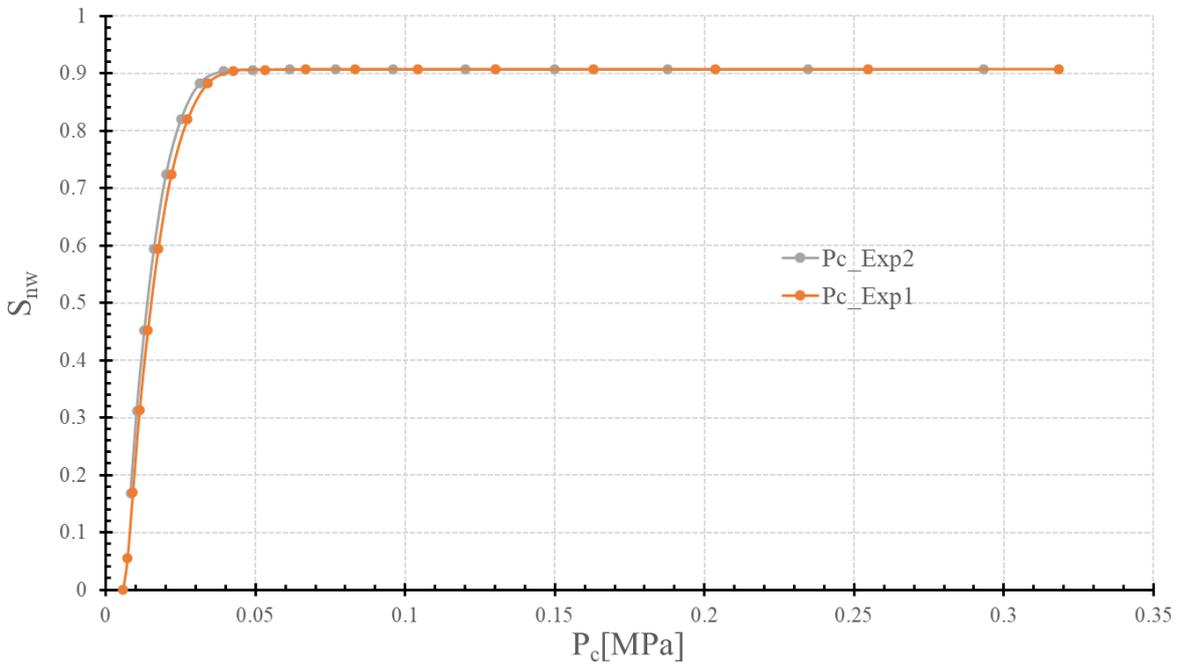

Figure 4-2. Capillary curves that include trapping for Exp1 and Exp2.

Berea *Stick and ball* model are visualized in Paraview. Since Paraview is not able to recognize throat properties, pores are visualized correctly in diameter, and throats are not. In this case, throats are visualized with a pore diameter property. Pore and throat diameter distributions are also visualized in Paraview Figure 4-4. and Figure 4-5., respectively. From these ranges, divided into 100 bins it is clear that throats prevail. Likewise, dense pore network model confirms it.
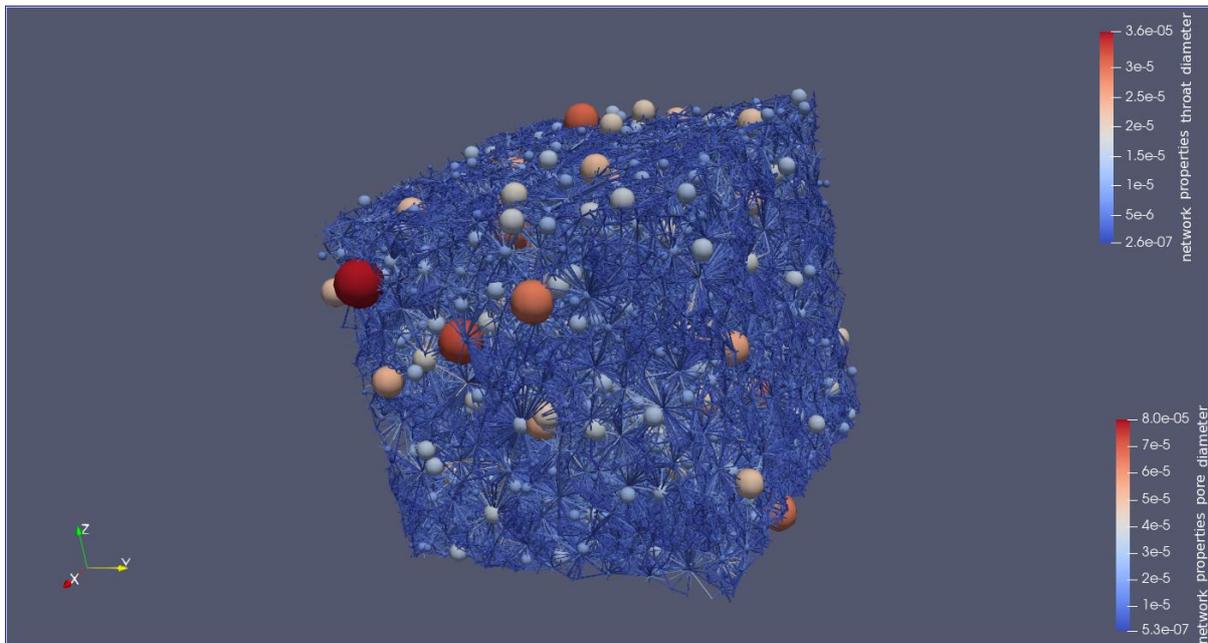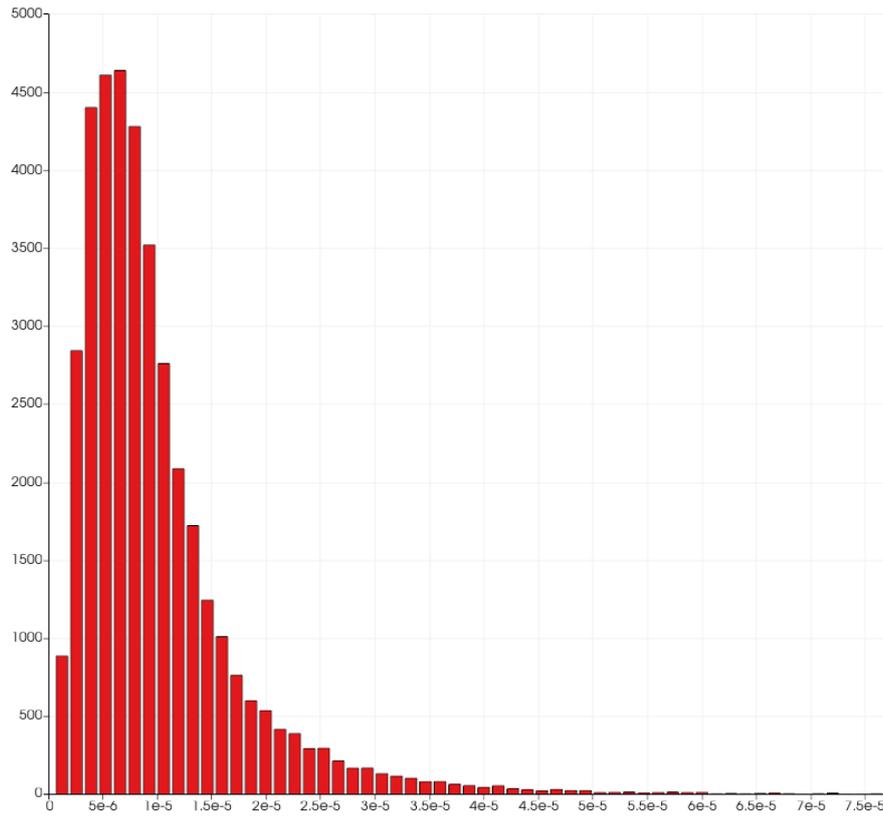

Figure 4-3. Stick and ball model of a Berea sandstone.

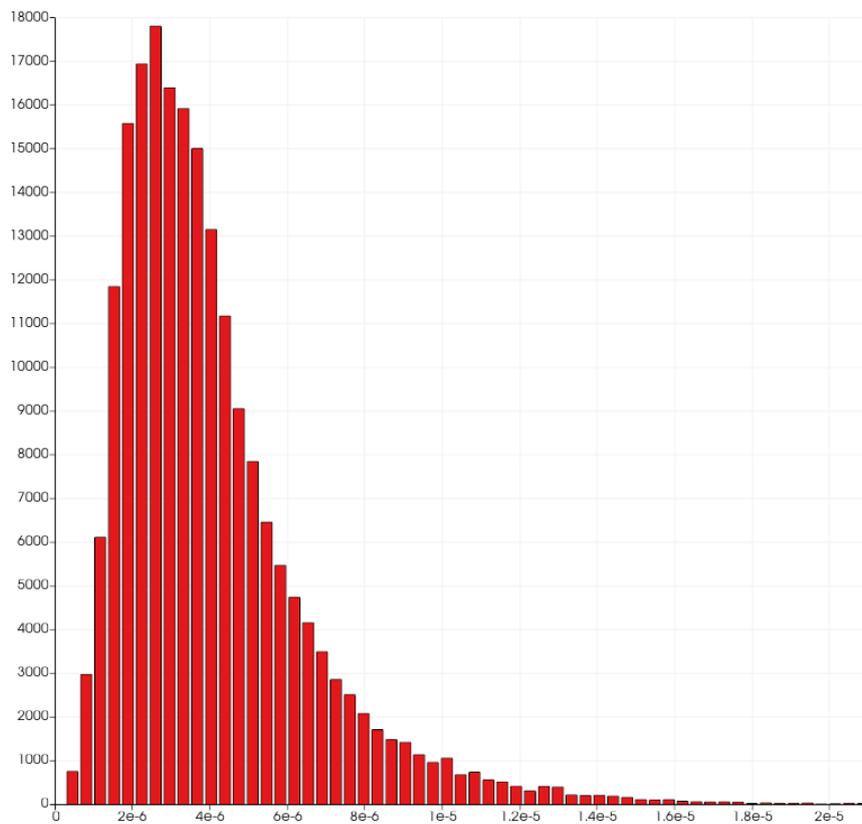**Figure 4-4**. Pore diameter distribution in meters divided in 100 bins.

Figure 4-5. Throat diameter distribution in meters divided in 100 bins.

4.2. Core scale

4.2.1 *Coreflood laboratory experiment*

The results were obtained from the aforementioned article. The porosity was uniform along the core axis and the average porosity was 17.6±0.2% (error) and is shown in Figure 4-6.(a) and (b). The pore volume of the core is obtained by multiplying the core's bulk volume by the average CT-measured porosity with the value of 429.3 mL. Figure 4-6.(c) shows the steady-state water saturation images for each step of the primary drainage for Exp5. Each step had lower f_w than the previous one. It is noticed that the steady-state S_w decreases as f_w decreases and that the S_w value near the core inlet is significantly lower at low f_w steps (f_w = 0.01, 0.001, 0).
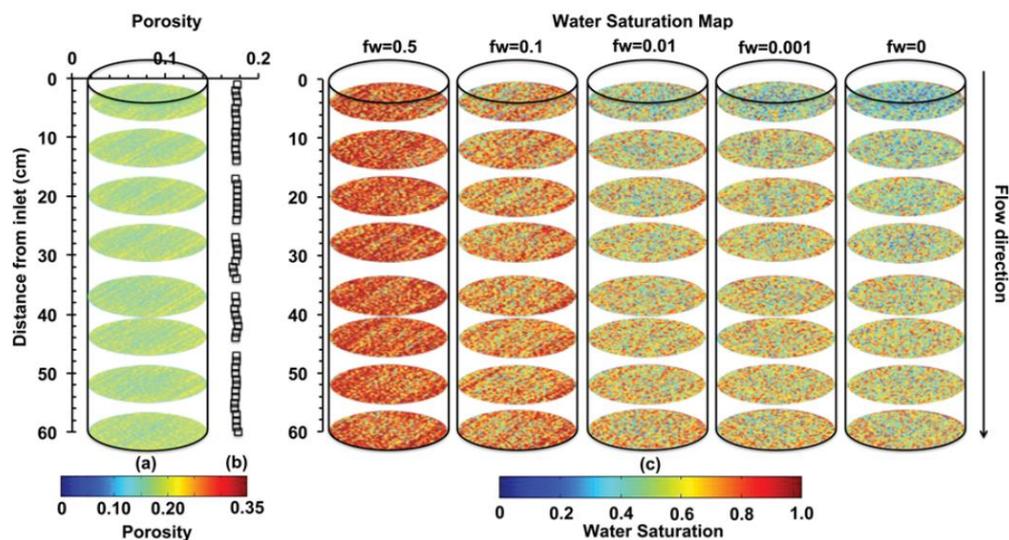

Figure 4-6. 1-cm thick slices of porosity images along the core axis (b) porosity profiles along core axis, (c) steady-state water saturation images along the core axis at every drainage step of primary drainage Exp5 (Chen et al., 2016).

In Figure 4-7. (Left), it can be clearly seen that the saturation mostly varies at the entrance and exit sections along the core axis at each injection stage. Taking an average of the obtained non-uniform saturations along the core may result in different relative permeabilities than the actual one. Additionally, if the saturation varies, the capillary pressure will also change. These two reasons are indicative why uniformity of saturation is important.

Normalized pressure gradient is calculated by multiplying the measured pressure gradient of each section by the absolute permeability of each section. Comparing the normalized

pressure gradients at steady state, which are roughly the same at each step in the center three middle sections, with uniform saturations in center sections, they were used to calculate CO_2-brine relative permeability. The capillary end effect can be clearly seen in the exit section, where normalized pressure gradients are twice as high (Figure 4-7. (Right)).
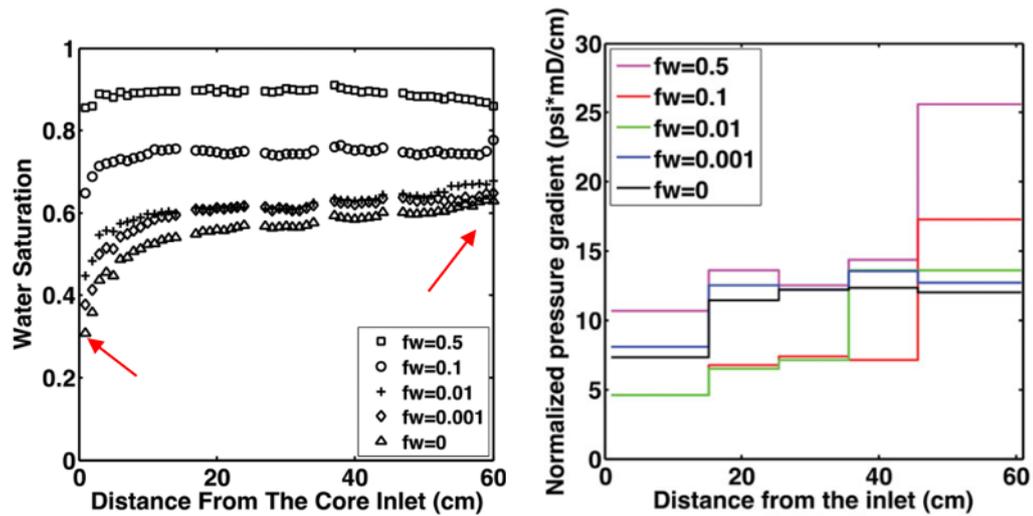

Figure 4-7. Steady state S_w profiles at different drainage steps (different f_w) in primary drainage Exp5 (Left). Normalized pressure gradient profiles at steady state for each fractional flow step in Exp5 (Right) (Chen et al., 2016).

In equations (3-15) and (3-16), Q_{CO2} and Q_{brine} are the flow rates of CO_2 and brine set by the pumps; μ_{CO2} and μ_{brine} are the viscosities of CO_2 (0.087 cp) and brine (1.081 cp); A is the cross section of the core (40.04 cm^2); ΔP_{nw} and ΔP_w are pressure drops of both phases; k_w is single phase permeability of the non-equilibrated brine which was measured before each primary drainage experiment; L is a length of the core. Difference in gravitational potential between the brine and CO_2 was only 1% of the typical overall pressure drop, and it can be therefore safely neglected.

Since the capillary pressure is the result of the interaction of two fluids with the rock, and it occurs inside the core, it is important to define which phase pressure is measured by the taps. Measured pressure drops in the center three sections are used to directly calculate both CO_2 and brine relative permeabilities with equations (3-15) and (3-16). These uncertainties are entirely due to fluctuations in the pressure drop. Inlet and outlet sections are more complicated simply because the Pc varies and the saturation is non-uniform. Therefore, section 1 measured pressure tap is used to calculate only the CO_2 relative permeability with equation (3-15). For

completeness, the pressure drop in section 5 (exit) was also used to calculate brine and CO_2 relative permeabilities, which shows how the capillary end effect underestimates the data.

Dashed and solid plotted lines in Figure 4-8. are Corey type models of relative permeabilities calculated using equations (3-17) and (3-18), while individual points represent steady-state relative permeabilities (experimental data). Exponents for Corey models, n_g and n_w were used as fitting parameters. Irreducible water saturation, S_{wi}, was averaged after each experiment. The resulting values are $S_{wi} = (26 \pm 2)$ %, $n_g = 1.8 \pm 0.1$, and $n_w = 5.2 \pm 0.3$. The uncertainty is mainly due to the scatter of the data.
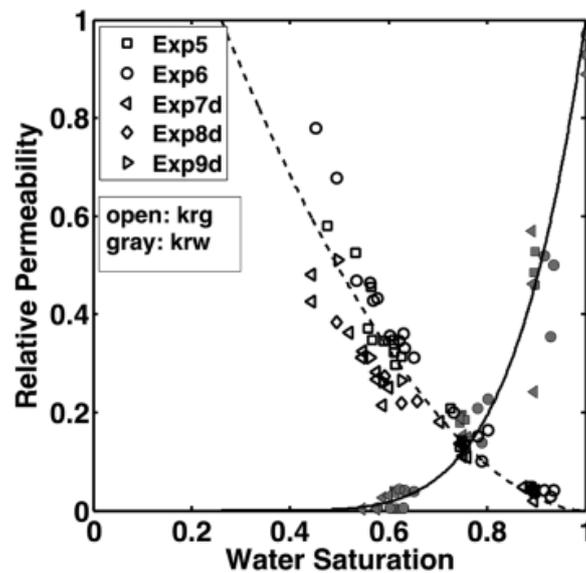

Figure 4-8. Steady-state CO_2 and brine relative permeabilities (from the entrance and the middle three sections) in all five primary drainage experiments (Chen et al., 2016).

Since the CO_2 relative permeabilities obtained from exit sections are roughly half the values throughout the whole core, they won't be considered in the final result. Nevertheless, it is important to understand and compare them with other studies. One of the solutions is to use bump flood test to achieve lower water saturation and higher CO_2 relative permeability, but these measurements only affect the endpoint CO_2. The second solution is to use longer cores and pressure taps, which is the simplest way. CO_2-brine relative permeabilities obtained in this article are higher than in other studies, but the data matches well with oil/water relative permeabilities in the same rock in Oak et al. (1990) study.

4.2.2. Coreflood numerical simulation

Steady state method in the simulation, requires restarting the simulation for each new water and CO_2 flow rate, which is the main reason unsteady state method is used more often. As mentioned previously, Chen et al. (2016), performed five primary drainage experiments. Their work showed that CO_2-brine relative permeabilities are similar to the Berea water-oil permeabilities, published by Oak et al. (1990). The measurements were made with simultaneous injection of brine and CO_2 in the so-called equilibrium phase. Although, in this part it is assumed that such mixtures are not needed, as the equilibrium of phases is the prerequisite of conservation of mass calculation at each iteration step in numerical simulation. They injected equilibrated CO_2, and equilibrated brine for fractional flows (at measurement p, T conditions): $f_w = 0$, $f_w = 0.001$, $f_w = 0.01$, $f_w = 0.1$, $f_w = 0.5$ and $f_w = 1$.

Results were compared to the Experiment number five (Exp5) from Chen et al. (2016). First, it is important to note that gravitational segregation of CO_2 and brine occurred, which is rather surprising for coreflood, however, it can be referred to horizontal flow direction (in opposite to the laboratory experiment, where the flow rate is vertical and the exit is on the bottom side).

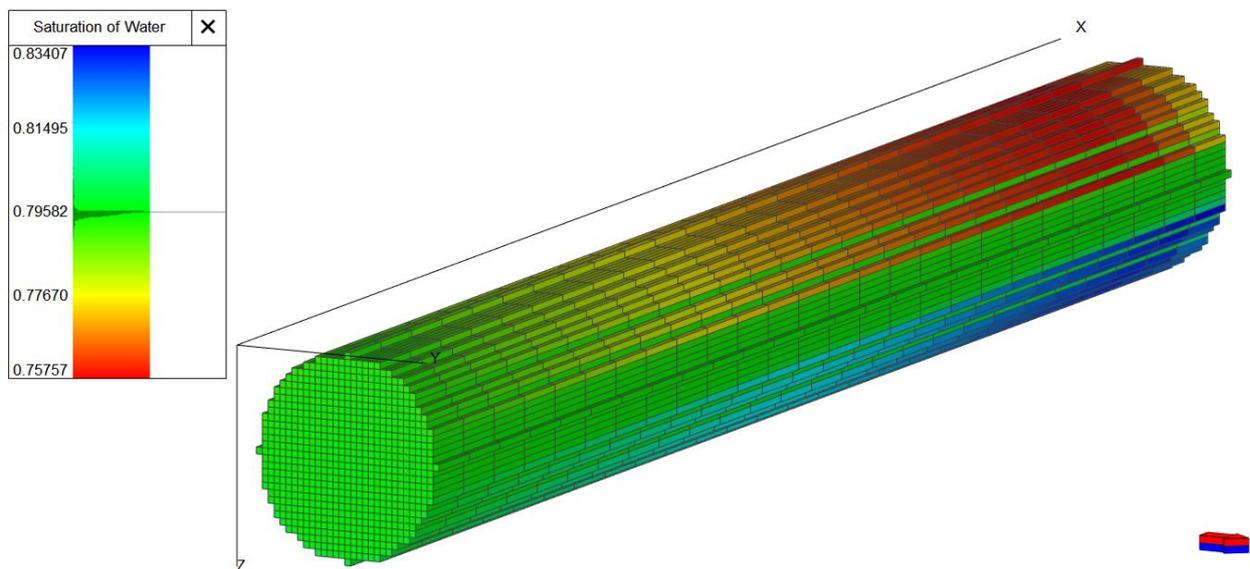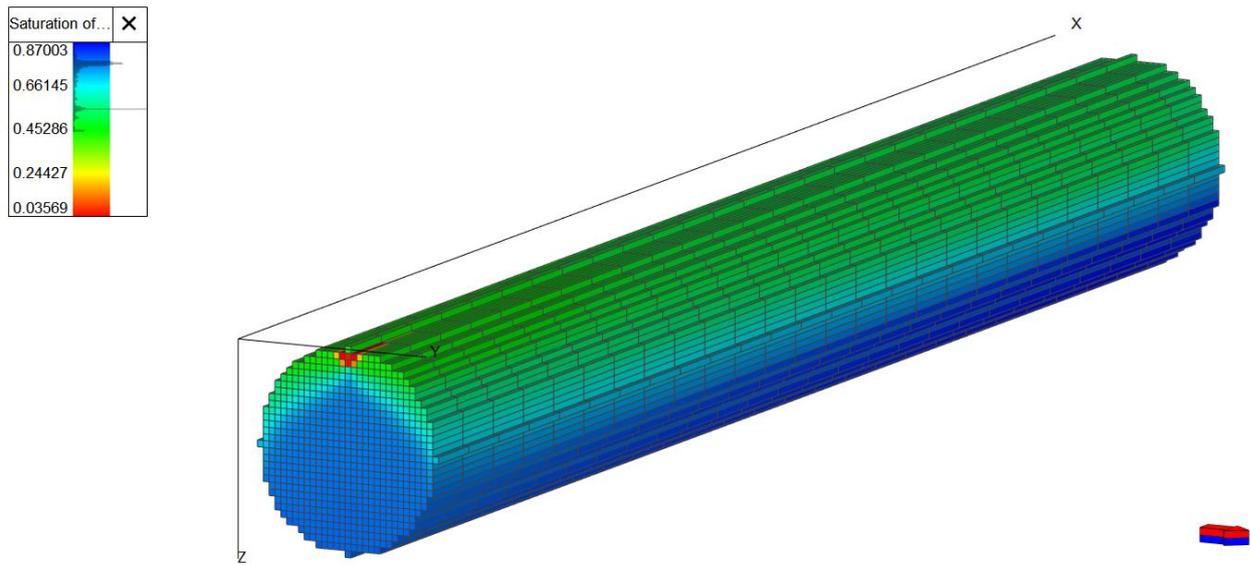**Figure 4-9**. Water saturation in core model at the end simulation for fw = 50 %.

Figure 4-10. Water saturation in core model at the end simulation for fw = 10 %.
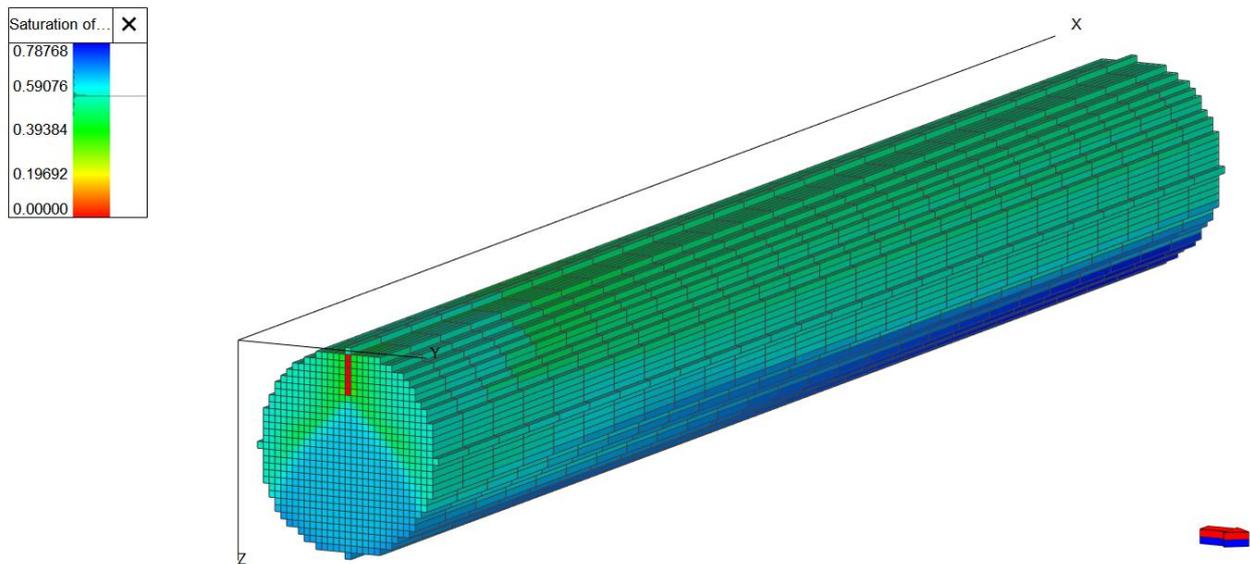
Figure 4-11. Water saturation in core model at the end simulation for fw = 1 %.
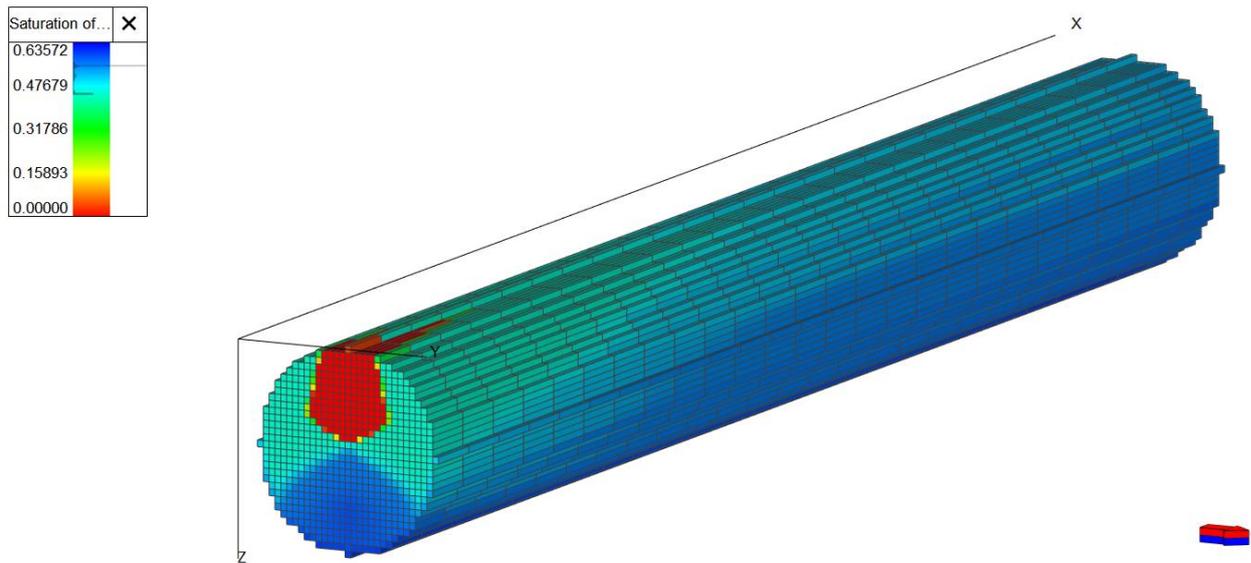
Figure 4-12. Water saturation in core model at the end simulation for fw = 0.1 %.

After that, the same experiment is simulated with capillary pressure modelled in PoreSpy ($P_c \neq$ 0, Figure 4-13., Figure 4-14., Figure 4-15. and Figure 4-16.).

Figure 4-13. Water saturation in core model at the end simulation for fw = 50 %, with capillary pressure table modelled with PoreSpy.

It is necessary to note that simulation runtime with P_c data included increases several times. For example, one run on Intel(R) Core(TM) i7-6700HQ CPU @ 2.60GHz without P_c (i.e. $P_c = 0$) takes about eight minutes, while with P_c table included the run for the same case takes about 55 minutes.

Considering this, the model with P_c shows the same objective results, but obviously more realistic saturation distribution. This is the moment when the amount of injected fluids (or duration of injection) was reconsidered as in the reference input data (Chen et al., 2016) it was assumed that during each injection flow rate, the steady state was achieved after less than 2 pore volumes (PV) for $f_w = 0.5, 0.1$, and about 5 PV for $f_w = 0.01, 0.001$ and 0. We used the criterion that steady state is obtained in simulation when the FWIP parameter (field water in place) no longer changes or varies by less than 0.1 ml every simulation time step, i.e. 10 minutes (less than 1 ml per hour). Figure 4-14. compares saturation ranges (and saturation distribution in a core after 2 PV are injected (43 timesteps = 7,16 hours with $f_w = 0.1$ set) as defined in reference, then after 10 hours (60 timesteps, as it was originally defined in coreflood model), and after no significant saturation change occurred (30 hours, 8,4 PV).
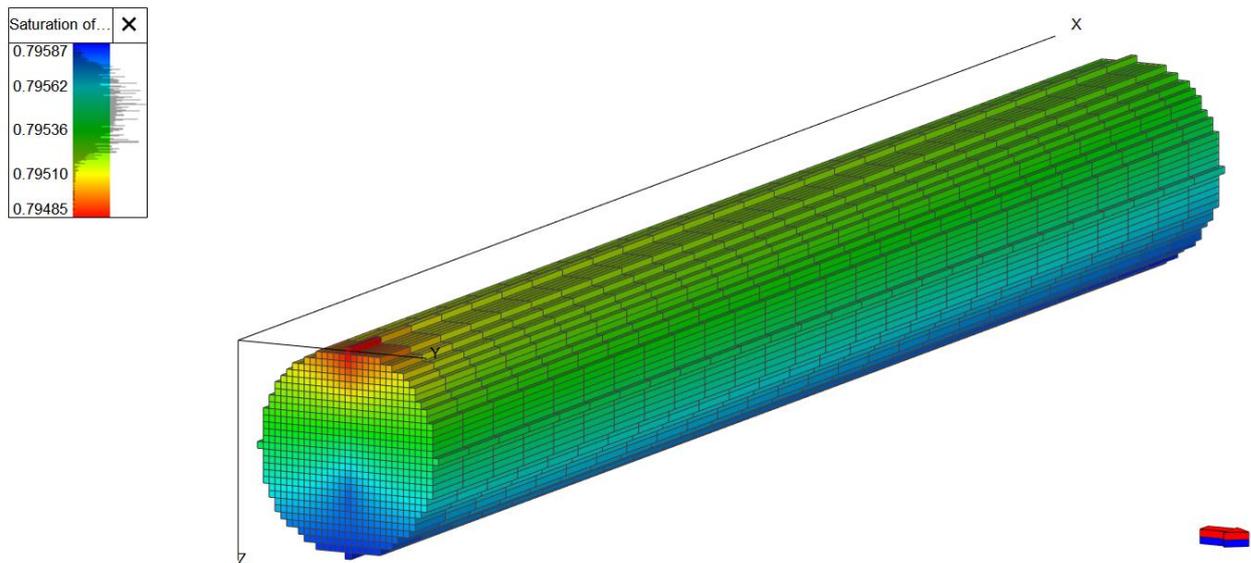
Figure 4-14. Water saturation in core saturation in core model at the end simulation for f_w = 10 %, with capillary pressure table modelled with PoreSpy and after 2 PV (7,16 hours), 2,8 PV (10 hours) and after 8,4 PV (30 hours, insignificant change in saturation).

Figure 4-15. Water saturation in core saturation in core model at the end simulation for $f_w = 1$ %, with capillary pressure table modelled with PoreSpy.

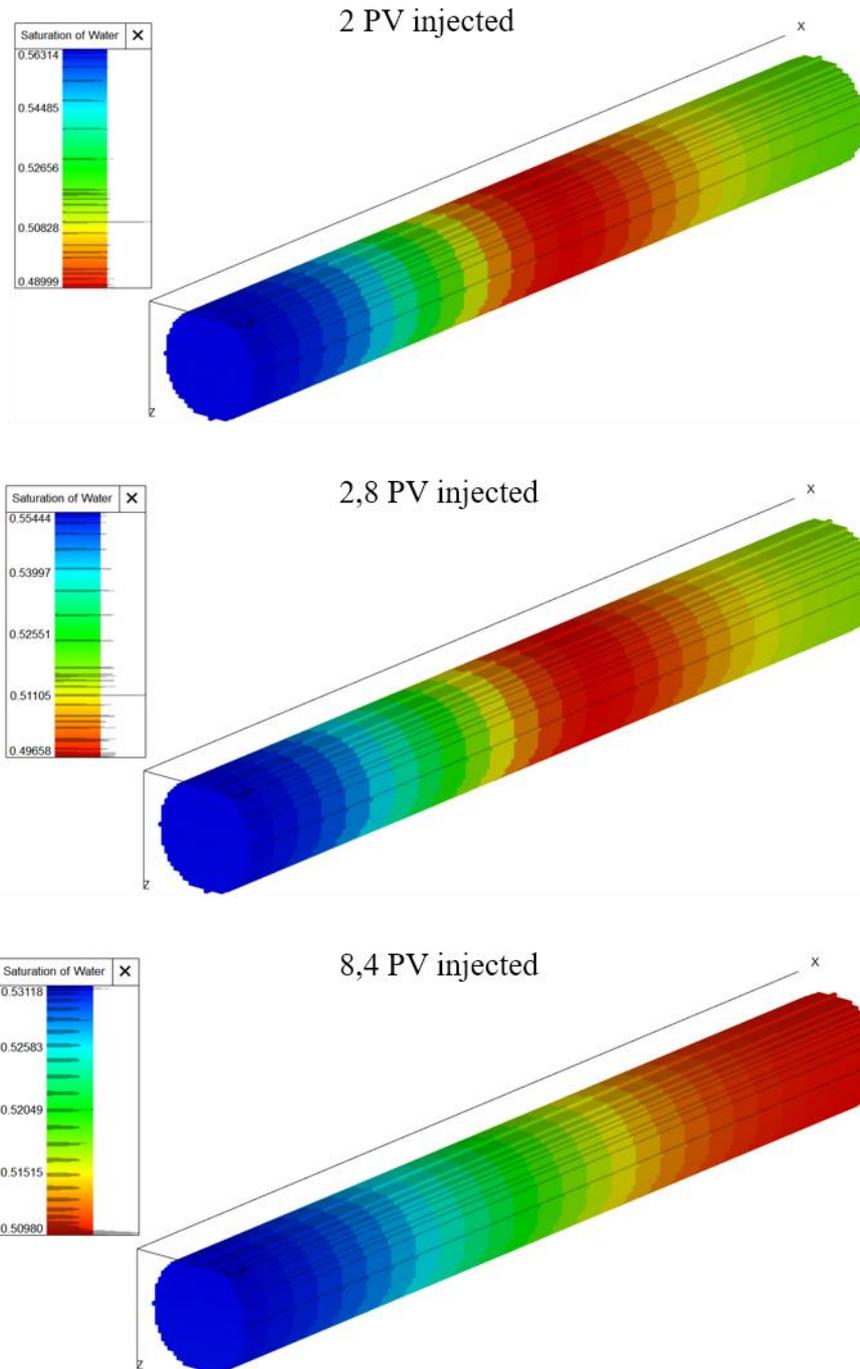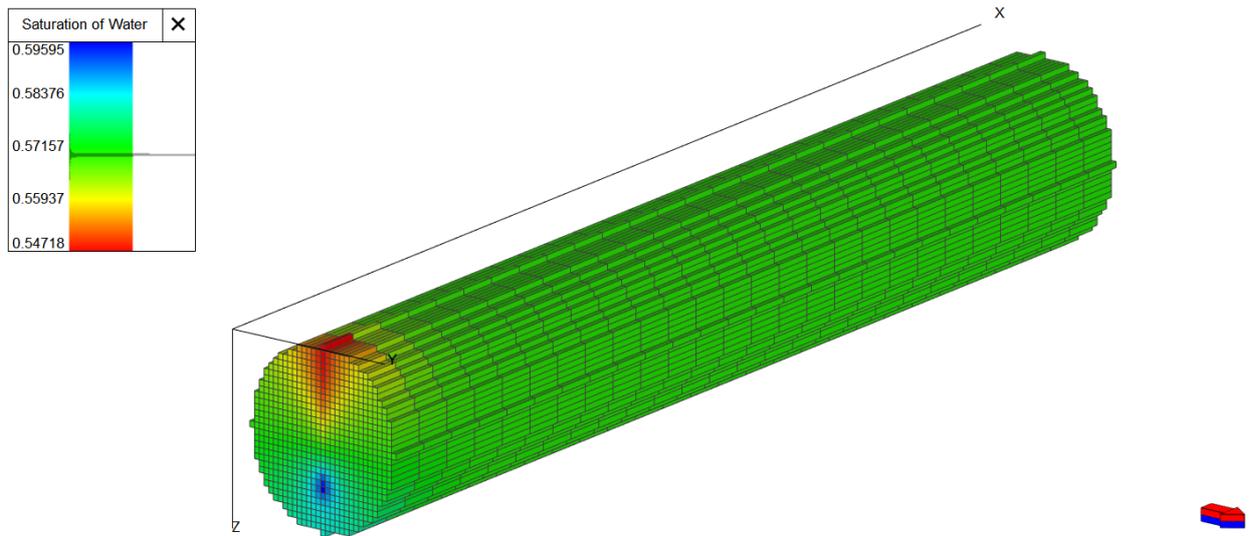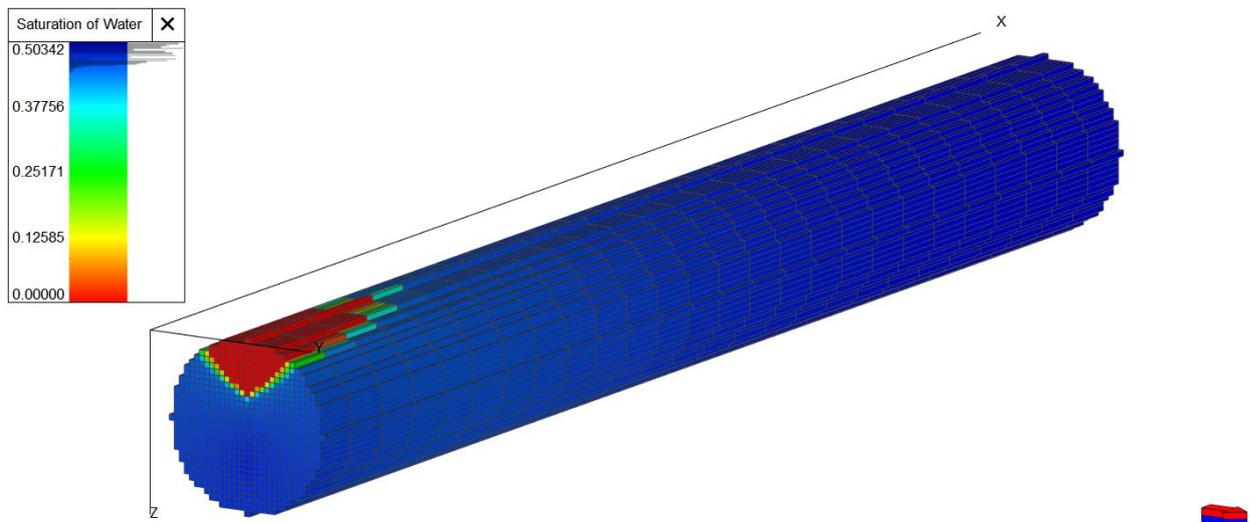**Figure 4-16**. Water saturation in core saturation in core model at the end simulation for $f_w = 0.1$ %, with capillary pressure table modelled with PoreSpy.

Relative permeability curves are presented on a single graph (Figure 4-17.) to compare all data available for further upscaling to reservoir scale (aquifer for CO_2 storage). Curves are fitted to Corey correlation, which provides consistency for full-scale simulations (Table 4-1.)
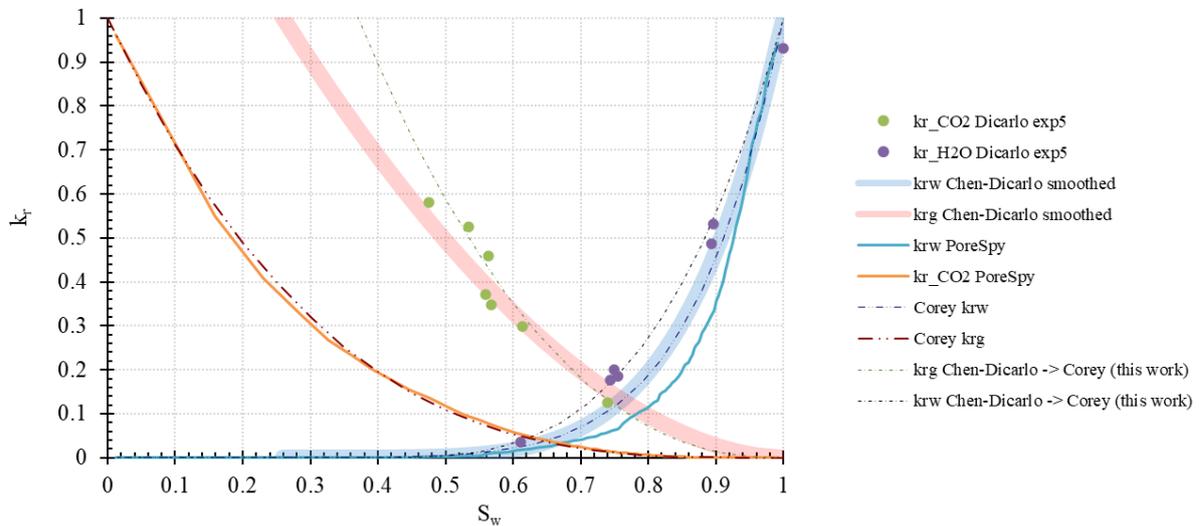
Figure 4-17. Available relative permeability data.

Table 4-1. Overview of Corey corelation parameters.

	PoreSpy	*Exp5*	*k_r smoothed*	*Corey from Chen and Dicarlo (2016)*
ng	3.2	2.3	2.3	1.8 +- 0.1
nw	7.5	3.4	4.5	5.2 +- 3
Siw	0	0.37	0.37	0.26+-0.02
Sgc	0	0	0	0
krg_cw	1	1	1	1
krw_gc	1	1	1	1

While data from Chen et al. (2016) are difficult to reproduce in coreflood simulation models, both datasets have drawbacks when smoothing using generalized Corey's correlation.

4.3. Reservoir scale

The simulation results of CO₂ injection into a deep saline aquifer. Eight simulation cases are compared to show the effects of different relative permeability on CO_2 storage (Table 4-2.). Besides relative permeability, only vertical permeability multiplier has been varied (two cases: $\frac{k_v}{k_h} = 0.5$ and $\frac{k_v}{k_h} = 0.1$).

Four relative permeability tables were used:

1. *krPoreSpy* is the same dataset as modeled with PoreSpy and tested in coreflood models.
2. *krPoreSpy-Corey*. The above dataset, *krPoreSpy*, has been fitted to Corey correlation parameters. It should be noted that only krPoreSpy (ad 1) provides capillary pressure data.
3. *krEXP5* represents the original experimental data from Chen et al. publication (2016).
4. *krChen-Corey* is a table of relative permeability derived using the Corey coefficients provided by Chen et al. (2016).

Table 4-2. Maximum pressure and plume migration after simulation with four relative permeability tables and two vertical permeability multipliers.

scenario	krPoreSpy	krPorespy-Corey	krEXP5	krChen-Corey	kh/kv	max. pressure at the end of injection (2045, bottom of reservoir)	max. plume spread	average aquifer pressure	FGIT	CO₂ stored
						bar	m	bar	10⁶ m³	Mt
1	1	0	0	0	0.5	519	1247	502	7165	13.4
2	0	1	0	0	0.5	522	1247	503	7137	13.3
3	0	0	1	0	0.5	518	1841	500	6980	13.1
4	0	0	0	1	0.5	521	1807	503	7183	13.4
5	1	0	0	0	0.1	520	1097	502	7180	13.4
6	0	1	0	0	0.1	521	1095	503	7162	13.4
7	0	0	1	0	0.1	520	1737	503	7131	13.3
8	0	0	0	1	0.1	521	1681	503	7325	13.7
					max	522	1841	503	7325	
					min	518	1095	500	6980	

Chen et al. (2016) results clearly highlight a difference in plume propagation from the injection well. Pressure during injection should be increased in the event of poor vertical permeability

(Figure 4-18., Figure 4-19.). Furthermore, the most critical zone during injection is the top (cap-rock) above the injection well, where pressure is fairly comparable to injection pressure (which is limited to 500 bar, and used for injection during most of injection time).

The plume is supposed to move faster to the shallower region of the layer when the vertical permeability is higher, especially if the layer is sloped. Capillary pressure seems to prevent the migration of CO_2 to shallower parts (Figure 4-20. and Figure 4-21.). It appears that capillary pressure effects dominanet after the injection, and that they influence the speed of plume migration, but not during the injection period (Figures 4-20. - 4-22.).
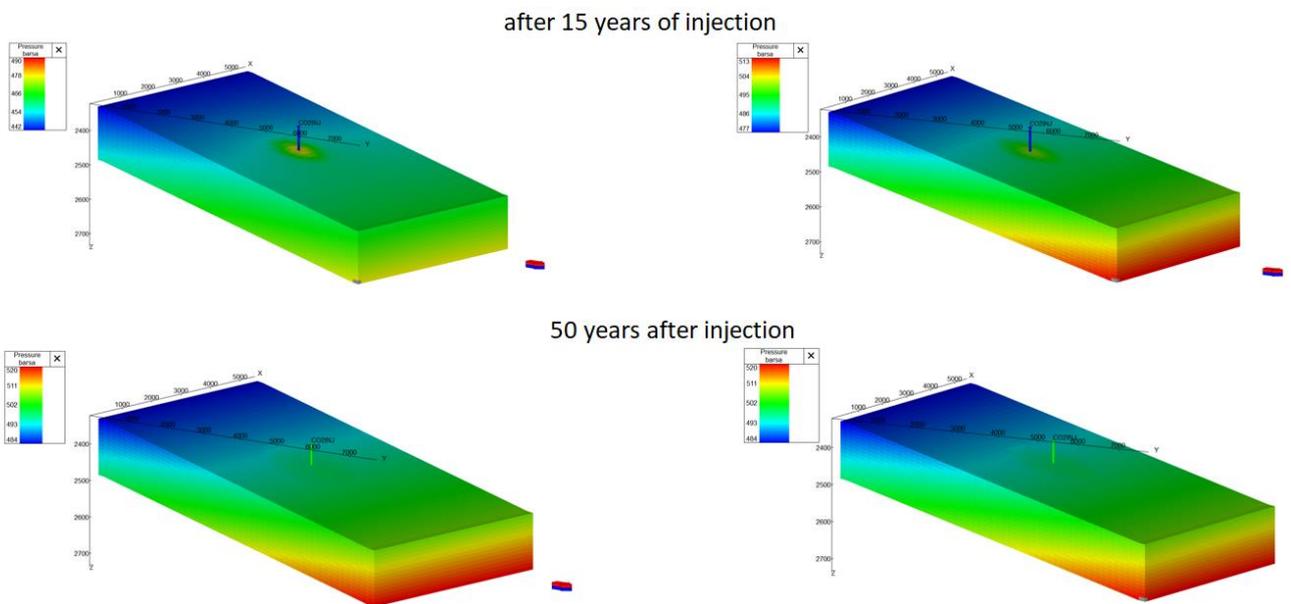

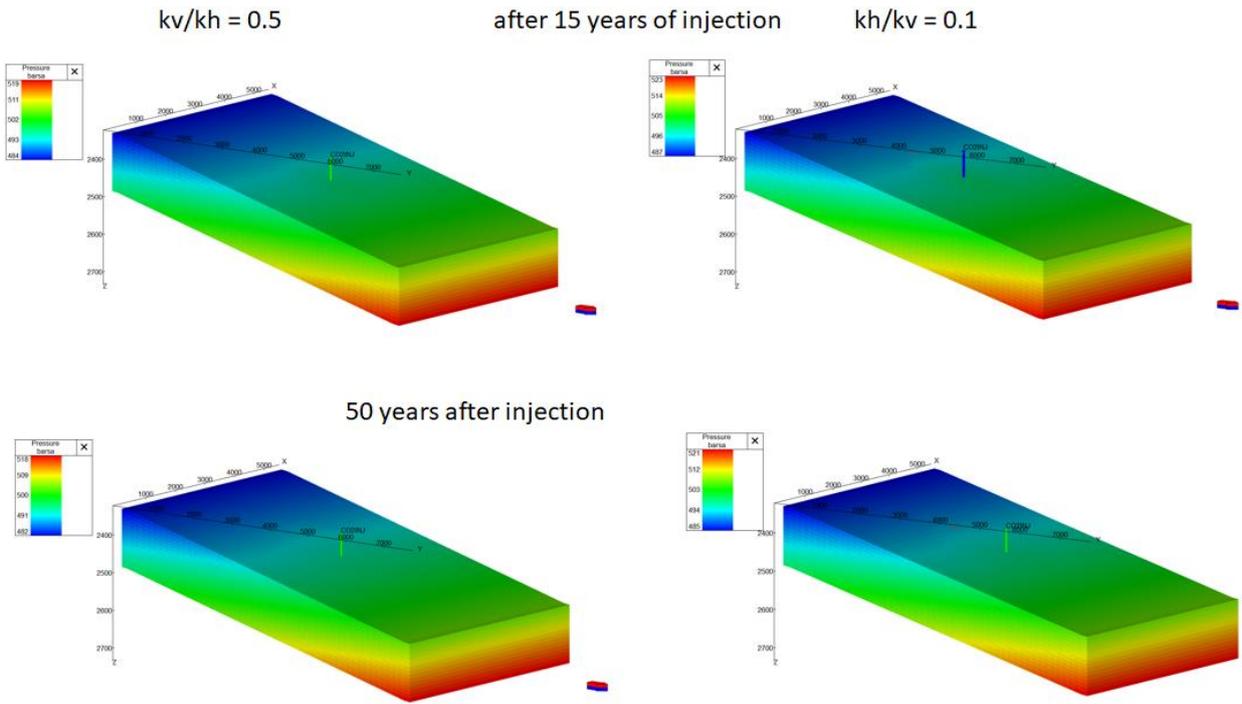**Figure 4-18**. PoreSpy case. Pressure distributions for k_v/k_h =0.5 (left) and k_v/k_h =0.1 (right).

Figure 4-19. PoreSpy case. Pressure distributions for k_v/k_h =0.5 and k_v/k_h =0.1.

Figure 4-20. Plume spread in the topmost layer at the end of the injection period and more than 50 after the injection for a PoreSpy case with capillary pressure included.

krPoreSpy-Corey, $k_v/k_h = 0.1$

2050. g. r_{max}=760.4 m

2100. g. r_{max}=1064.6 m

krPoreSpy-Corey, $k_v/k_h = 0.5$

2050. g. r_{max}=912.5 m
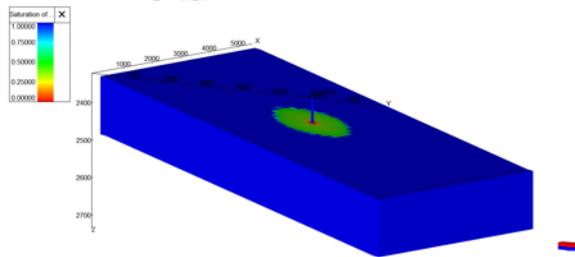
2100. g. r_{max}=1064 m

Figure 4-21. Plume spread in the topmost layer at the end of the injection period and more than 50 after the injection for a PoreSpy case without capillary pressure included.

exp5, $k_v/k_h = 0.1$

plume spread

2050. g. r_{max}=1373 m

2100. g. r_{max}=1828 m

exp5, $k_v/k_h = 0.5$

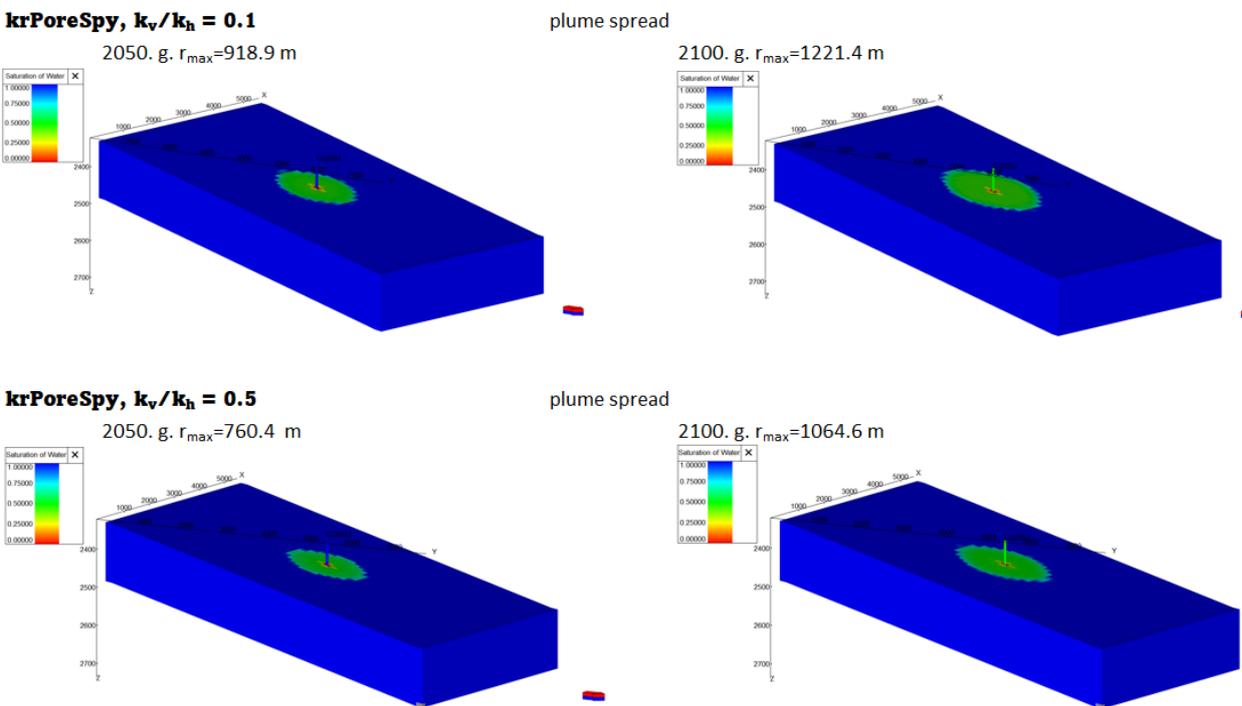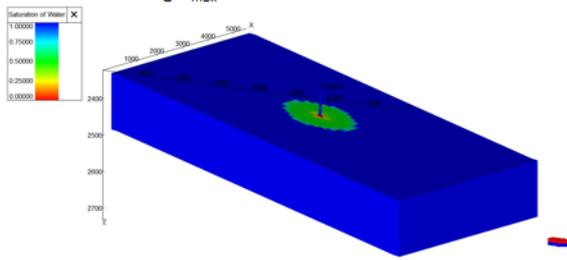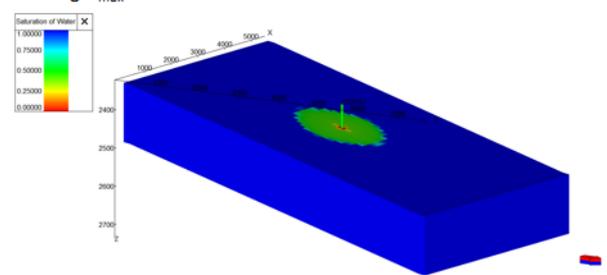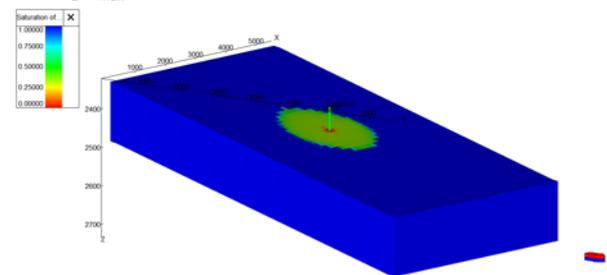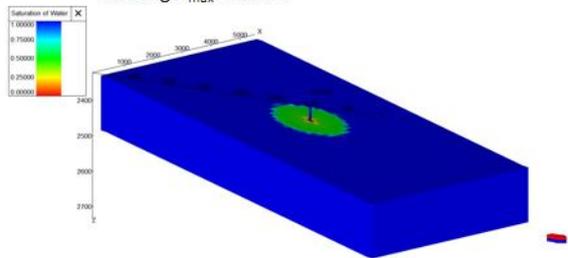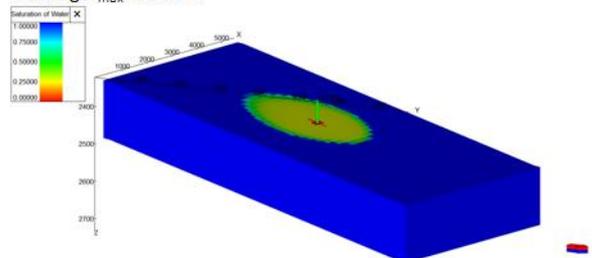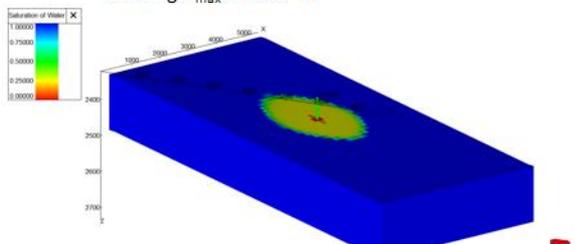plume spread

2050. g. r_{max}=1368.7 m
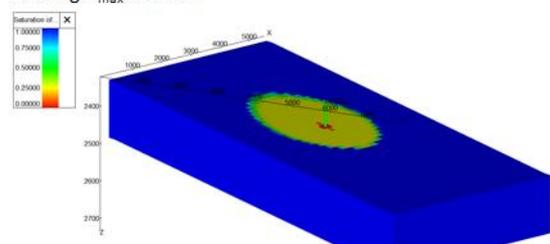
2100. g. r_{max}=1825 m

Figure 4-22. Plume spread in the topmost layer at the end of the injection period and more than 50 after the injection for a exp5 case (k_r from Chen et al., 2016) without capillary pressure included.

5. DISCUSSION

After the steady state is achieved, core exhibits feature that higher water saturation is present at the beginning of the core. This could be addressed to capillary end effect at the inlet and outlet of the core, which confirms that tNavigator can realistically describe fluid flow behaviour determined by pore-scale effects.

In the reference data from Chen et al. (2016) far less PV of brine and CO_2 were cumulatively injected at given pressure and temperature conditions, which can be explained by the fact that such a long laboratory analysis time for a single coreflood test is unacceptable. Another issue could be the precision of the instrument, including signal noise in a logger (since volume readings in a log are likely to be volatile, so the average trend in a given time range could be taken).

Both the data from this pore-scale (PoreSpy) analysis upscaled to the coreflood model, and the data from Chen et al. (2016) leave a large degree of freedom for reservoir simulation modeling, thus leading to the recommendation that uncertainties of CO2 storage simulation should be represented as a function of relative permeabilities, which is more scalable by using Corey's coefficients.

Reservoir scale simulations show the magnitude of influence of relative permeability and capillary pressure data on plume migration. It is shown how data from the same rock type (Berea sandstone) can be used and result in significantly different reservoir behaviours during and after the injection. It should be noted at this point that plume migrates after injection, and that in real cases of CO_2 storage, 4D monitoring of plume migration is required long after injection. At this point we introduce a 50-year plume increase coefficient ($pic_{50} = r_{pmax_{dyn}}/r_{pmax_{stat50}}$), where $r_{pmax_{dyn}}$ stands for maximum plume radius from the injection well shortly after well shutdown and $r_{pmax_{stat50}}$ stands for maximum plume radius from the injection well, fifty years after $r_{pmax_{stat50}}$ is achieved (Table 5-1.). It shows how the maximum radius of CO_2 saturation (from injection well) in a fifty-year period after injection stopped, and in this study $pic_{50} = 17\ to\ 50$ %. Fifty years is very likely time set for mandatory monitoring in legal acts. Another parameter was introduced to quantify plume migration (spreading) rate $pmr = (r_{pmax_{t1}} - r_{pmax_{t2}})/(t_2 - t_1)$ (m/y), where $r_{pmax_{t1}}\ and\ r_{pmax_{t2}}$ are maximum plume radius at years t_1 and t_2 respectively.

Table 5-1. Summary of plume migration benchmarks.

simulation case name	k_h/k_v	plume spread 2050	plume spread 2100	increase pic$_{50}$	plume migration rate pmr
krPoreSpy	0.1	918	1097	1.19	3.6
krPoreSpy	0.5	949	1247	1.31	6.0
krExp5	0.1	1287	1737	1.35	9.0
krExp5	0.5	1424	1841	1.29	8.3
krPorespy-Corey	0.1	931	1095	1.18	3.3
krPorespy-Corey	0.5	943	1247	1.32	6.1
krChen-Corey	0.1	1261	1681	1.33	8.4
krChen-Corey	0.5	1347	1807	1.34	9.2

To test whether *pmr* can be used to extrapolate the plume maximum radius, two models were simulated 250 years after the injection stopped krPoreSpy2 and krChen-Corey2 (with conservative $k_v/k_h = 0.1$, Figure 5-2.).
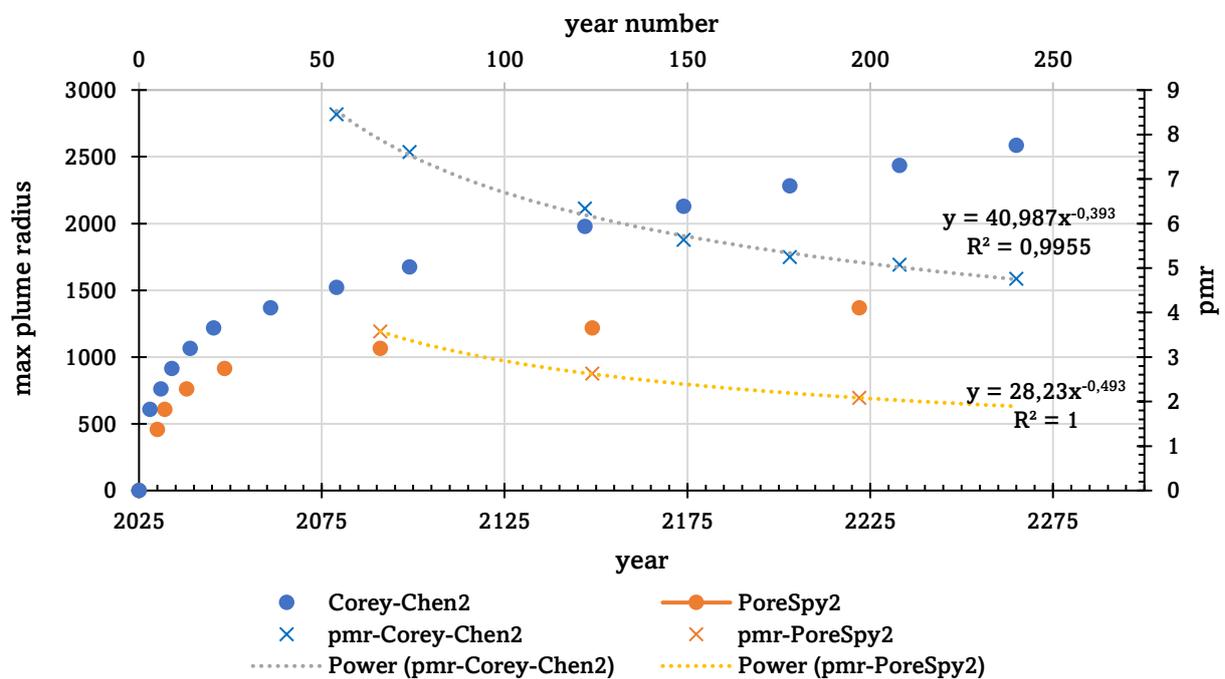

Figure 5-1. Plume migration 250 years after the injection.

6. CONCLUSION

The workflow, which includes experimental and numerical methods, is presented for each upscaling part from pore network modeling, coreflood experiment, and simulation of CO_2 injection into a deep saline aquifer. Based on the obtained results, following conclusions are drawn:

- A thorough geological model, including grid refinement to precisely predict plume migration rate, is necessary to correlate plume movement following injection.

- A simulation of 250 years after the injection ended shows that the plume would move until it reaches the top of the structure, which was not the case in this study because the injection well was placed in the middle of the model.

- Obtaining high resolution images from microtomography, certainly ensures representative background for further rock imaging tools. The OpenPNM module demonstrated the ability to extract the pore network.

- PoreSpy module provides precise pore-scale data (for a large number of saturation points) and consequently provides similar results to those obtained with smoothed data (Corey or similar correlation type). For further study, pore and throat size distribution should be taken into consideration to estimate capillary pressure better.

- Based on the consistency of parameters at all scales, it shows the potential of this upscaling approach. The PoreSpy module itself should be improved for better determination of critical saturation properties (usually, residual saturations do not exist, or are too small numbers).

A comparison of data obtained at all scales (pore scale, core scale, and reservoir scale) reveals that smoothed relative permeability curves (such as those matched with Corey's correlation) have no significant effect on the final simulation results (at reservoir scale). That is, the benefit of DRP should be utilized in such a way that a large number of observations of relative permeability and capillary pressure are made. Such an approach requires a systematic workflow for data storage, image segmentation, and binarized image analysis, as well as comparison of results at the core scale, in order to provide a statistically significant sample of saturation table datasets and a justified selection of P_c and k_r data that influence CO_2 plume dynamics and CO_2 injection features at realistic geological CO_2 storage candidates.

7. REFERENCES

1. ARNAUT, M., VULIN, D., JOSÉ GARCÍA LAMBERG, G. AND JUKIĆ, L., 2021. Simulation analysis of CO2-EOR process and feasibility of CO2 storage during EOR. *Energies*, *14*(4), p.1154.

2. BARKER, J. W., & THIBEAU, S., 1997. A critical review of the use of pseudorelative permeabilities for upscaling. *SPE Reservoir Engineering*, *12*(02), 138-143. DOI: https://doi.org/10.2118/35491-PA

3. BLUESCIENTIFIC, 2021. URL: https://blue-scientific.com/bruker-micro-ct/micro-ct-geology/

4. BLUNT, M. J., BIJELJIC, B., DONG, H., GHARBI, O., IGLAUER, S., MOSTAGHIMI, P., ... & PENTLAND, C., 2013. Pore-scale imaging and modelling. *Advances in Water resources*, *51*, 197-216. DOI: https://doi.org/10.1016/j.advwatres.2012.03.003

5. BRUKER, 2023. URL: https://www.bruker.com/en/products-and-solutions/preclinical-imaging/micro-ct.html

6. CHEN, X., KIANINEJAD, A., & A. DICARLO, D., 2016. Measurements of CO2-brine relative permeability in Berea sandstone using pressure taps and a long core. *Greenhouse Gases: Science and Technology*, *7*(2), 370-382. DOI: https://doi.org/10.1002/ghg.1650

7. CHURCHER, P. L., FRENCH, P. R., SHAW, J. C., & SCHRAMM, L. L. February, 1991. Rock properties of Berea sandstone, Baker dolomite, and Indiana limestone. In *SPE international symposium on oilfield chemistry*, OnePetro. DOI: https://doi.org/10.2118/21044-MS

8. DONG, H., & BLUNT, M. J., 2009. Pore-network extraction from micro-computerized-tomography images. *Physical review E*, *80*(3), 036307. DOI: http://dx.doi.org/10.1103/PhysRevE.80.036307

9. DUNSMUIR, J. H., FERGUSON, S. R., D'AMICO, K. L., & STOKES, J. P., 1991, October. X-ray microtomography: a new tool for the characterization of porous media. In *SPE annual technical conference and exhibition*. OnePetro. DOI: https://doi.org/10.2118/22860-MS

10. ESPINOZA, D. N., & SANTAMARINA, J. C., 2010. Water-CO2-mineral systems: Interfacial tension, contact angle, and diffusion—Implications to CO2 geological storage. *Water resources research*, *46*(7). DOI: https://doi.org/10.1029/2009WR008634

11. GOSTICK, J. T., 2017. Versatile and efficient pore network extraction method using marker-based watershed segmentation. *Physical Review E*, *96*(2), 023307. DOI: https://doi.org/10.1103/PhysRevE.96.023307

12. GUO, H., SONG, K., & HILFER, R., 2022. A Brief Review of Capillary Number and its Use in Capillary Desaturation Curves. *Transport in Porous Media*, *144*(1), 3-31. DOI: https://doi.org/10.1007/s11242-021-01743-7

13. HAERI, F., TAPRIYAL, D., SANGUINITO, S., SHI, F., FUCHS, S. J., DALTON, L. E., ... & GOODMAN, A., 2020. CO2–brine contact angle measurements on Navajo, Nugget, Bentheimer, Bandera brown, Berea, and Mt. Simon sandstones. *Energy & Fuels*, *34*(5), 6085-6100. DOI: https://doi.org/10.1021/acs.energyfuels.0c00436

14. HASSANIZADEH, S. M., & DAS, D. B., 2005. *Upscaling multiphase flow in porous media: from pore to core and beyond*. Springer.

15. JEONG, G. S., KI, S., LEE, D. S., & JANG, I., 2021. Effect of the Flow Rate on the Relative Permeability Curve in the CO2 and Brine System for CO2 Sequestration. Sustainability 2021, 13, 1543. DOI: 10.3390/su13031543

16. JUKIĆ, L., VULIN, D., LUKIĆ, M. AND SEDLAR, D.K., 2022. Enhanced gas recovery and storability in a high CO2 content gas reservoir. International Journal of Greenhouse Gas Control, 117, p.103662.

17. MAHDIABAD, O. A., 2020. *Primary drainage in static pore network modelling: a comparative study* (Doctoral dissertation, University of Leoben).

18. NIST, 2021. URL: https://webbook.nist.gov/chemistry/fluid/

19. OAK, M. J., BAKER, L. E., & THOMAS, D. C., 1990. Three-phase relative permeability of Berea sandstone. *Journal of Petroleum Technology*, *42*(08), 1054-1061. DOI: https://doi.org/10.2118/17370-PA

20. OPENPNM, 2023. URL: https://openpnm.org/index.html

21. ØREN, P. E., & BAKKE, S., 2002. Process based reconstruction of sandstones and prediction of transport properties. *Transport in porous media*, *46*(2-3), 311-343. DOI: https://doi.org/10.1023/A:1015031122338,

22. PICKUP, G. E., STEPHEN, K. D., MA, J., ZHANG, P., & CLARK, J. D., 2005. Multi-stage upscaling: Selection of suitable methods. *Transport in porous media*, *58*, 191-216. DOI: https://doi.org/10.1007/s11242-004-5501-5

23. PORESPY, 2023. URL: https://porespy.org/index.html

24. POULSEN, N., BOCIN-DUMITRIU, A., HOLLOWAY, S., KIRK, K., NEELE, F., & SMITH, N., 2015. Reserves and resources for CO_2 storage in Europe: the CO2StoP project. *GEUS Bulletin*, 33, 85–88. DOI: https://doi.org/10.34194/geusb.v33.4516

25. RABBANI, A., JAMSHIDI, S., & SALEHI, S., 2014. An automated simple algorithm for realistic pore network extraction from micro-tomography images. *Journal of Petroleum Science and Engineering*, *123*, 164-171. DOI: https://doi.org/10.1016/j.petrol.2014.08.020

26. ROCK FLOW DYNAMICS, 2022. tNavigator 21.4. Simulation User Manual, Rock Flow Dynamics, Houston, USA

27. SAFTIĆ, B., KOLENKOVIĆ MOČILAC, I., CVETKOVIĆ, M., VULIN, D., VELIĆ, J. AND TOMLJENOVIĆ, B., 2019. Potential for the Geological Storage of CO2 in the Croatian Part of the Adriatic Offshore. *Minerals*, *9*(10), p.577.

28. SHEPPARD, A. P., SOK, R. M., AVERDUNK, H., ROBINS, V. B., & GHOUS, A., 2006, September. Analysis of rock microstructure using high-resolution X-ray tomography. In *Proceedings of the International Symposium of the Society of Core Analysts* (pp. 1-12). Dublin, Ireland: The Society of Core Analysts.

29. SPANNE, P., THOVERT, J. F., JACQUIN, C. J., LINDQUIST, W. B., JONES, K. W., & ADLER, P. M., 1994. Synchrotron computed microtomography of porous media: topology and transports. *Physical review letters*, *73*(14), 2001. DOI: https://doi.org/10.1103/PhysRevLett.73.2001

30. SUŠILOVIĆ, N., 2020. *Mogućnosti digitalne analize svojstava stijena korištenjem OpenPNM i PoreSpy Python modula* (Bachelor's Thesis, University of Zagreb. Faculty of Mining, Geology and Petroleum Engineering. Department of Petroleum and Gas Engineering and energy). DOI: urn:nbn:hr:169:922581

31. THOMPSON, K. E., WILLSON, C. S., WHITE, C. D., NYMAN, S., BHATTACHARYA, J. P., & REED, A. H., 2008. Application of a new grain-based reconstruction algorithm to microtomography images for quantitative characterization and flow modeling. *Spe Journal*, *13*(02), 164-176. DOI: https://doi.org/10.2118/95887-PA

32. VALVATNE, P. H., PIRI, M., LOPEZ, X., & BLUNT, M. J., 2005. Predictive pore-scale modeling of single and multiphase flow. *Upscaling Multiphase Flow in Porous Media: From Pore to Core and Beyond*, 23-41. DOI: 10.1007/1-4020-3604-3_3

33. VANGKILDE-PEDERSEN, T., ANTHONSEN, K.L., SMITH, N., KIRK, K., VAN DER MEER, B., LE GALLO, Y., BOSSIE-CODREANU, D., WOJCICKI, A., LE NINDRE, Y.M., HENDRIKS, C. AND DALHOFF, F., 2009. Assessing European capacity for geological storage of carbon dioxide–the EU GeoCapacity project. *Energy Procedia*, 1(1), pp.2663-2670. DOI: https://doi.org/10.1016/j.egypro.2009.02.034

34. VANGKILDE-PEDERSEN, T., KIRK, K., SMITH, N., MAURAND, N., WOJCICKI, A., NEELE, F., HENDRIKS, C., LE NINDRE, Y. AND LYNG ANTHONSEN, K., 2009. EU GeoCapacity–Assessing European Capacity for Geological Storage of Carbon Dioxide. *Project no. SES6-518318*. DOI: https://cordis.europa.eu/project/id/518318/reporting

35. VULIN, D., MUHASILOVIĆ, L. AND ARNAUT, M., 2020. Possibilities for CCUS in medium temperature geothermal reservoir. *Energy*, *200*, p.117549.

36. VULIN, D., SAFTIĆ, B. AND MACENIĆ, M., 2018. Estimate of dynamic change of fluid saturation during CO_2 injection—Case study of a regional aquifer in Croatia. *Interpretation*, *6*(1), pp. 51-64.

8. APPENDIX

1. PoreSpy simulation

```python
# Importing packages
import os
import imageio
import numpy as np
import matplotlib.pyplot as plt, numpy as np
from mpl_toolkits.mplot3d import Axes3D
import numpy as np
import porespy as ps
import openpnm as op
import matplotlib.pyplot as plt


# Importing image
path='C:\\Users\\Nikolina\\Desktop\\Python programi\\'
file_format = '.tif'
file_name = 'Berea_sample_800x800x800'
file = file_name + file_format
fetch_file = os.path.join(path, file)
im = imageio.mimread(fetch_file, memtest=False)
im = ~np.array(im, dtype=bool)
import random
np.random.seed(0)


# Pore network extraction using SNOW algoritm
snow = ps.networks.snow2(
    phases=im,
    phase_alias={True:"void",False:"solid"},
    voxel_size=1.5e-06)

ws = op.Workspace()
pn = op.io.network_from_porespy(snow.network)
pn.add_model_collection(op.models.collections.geometry.spheres_and_cylinders)
pn.regenerate_models()
proj = pn.project

# Add boundary pores from extracted network
min_coor = pn['pore.coords'].min()
max_coor = pn['pore.coords'].max()

def marker_arr(min_value,max_value,boundary='left'):

    if boundary == 'left':
        marker = [
                min_value,
                random.uniform(min_value,max_value),
                random.uniform(min_value,max_value)
                ]

    if boundary == "right":
        marker = [
        max_value,
        random.uniform(min_value,max_value),
        random.uniform(min_value,max_value)
```

```python
        ]

    return marker

left_marker = [marker_arr(min_coor,max_coor) for _ in range(20)]
right_marker = [marker_arr(min_coor,max_coor,'right') for _ in range(20)]
left_marker = np.array(left_marker)
right_marker = np.array(right_marker)

op.topotools.find_surface_pores(network=pn, markers=left_marker, label='left')
op.topotools.find_surface_pores(network=pn, markers=right_marker, label='right')

# Invasion Percolation
air = op.phase.Air(network=pn,name='air')
air['pore.contact_angle'] = 30
air['throat.contact_angle'] = 30
air['pore.surface_tension'] = 0.035
air['throat.surface_tension'] = 0.035
air['pore.density'] = 850
air['throat.density'] = 850
air['pore.viscosity'] = 0.087E-3
air['throat.viscosity'] = 0.087E-3
air.add_model_collection(op.models.collections.phase.air)
air.add_model_collection(op.models.collections.physics.basic)
air.regenerate_models()

water = op.phase.Water(network=pn,name='water')
water['pore.contact_angle'] = 150
water['throat.contact_angle'] = 150
water['pore.surface_tension'] = 35e-3
water['throat.surface_tension'] = 35e-3
water['pore.density'] = 1000
water['throat.density'] = 1000
water['pore.viscosity'] = 1.08E-3
water['throat.viscosity'] = 1.08E-3
water.add_model_collection(op.models.collections.phase.water)
water.add_model_collection(op.models.collections.physics.basic)
water.regenerate_models()

ip = op.algorithms.InvasionPercolation(network=pn, phase=air)
Finlets_init = pn.pores('left')
Finlets=([Finlets_init[x] for x in range(0, len(Finlets_init), 2)])
ip.set_inlet_BC(pores=Finlets)
ip.run()

# Kr simulation
def sat_occ_update(network, nwp, wp, ip, i):
    r"""
        Calculates the saturation of each phase using the invasion
        sequence from either invasion percolation.
        Parameters
        ----------
        network: network
        nwp : phase
            non-wetting phase
        wp : phase
            wetting phase
```

```
        ip : IP
            invasion percolation (ran before calling this function)
        i: int
            The invasion_sequence limit for masking pores/throats that
            have already been invaded within this limit range. The
            saturation is found by adding the volume of pores and thorats
            that meet this sequence limit divided by the bulk volume.
    """
    pore_mask = ip['pore.invasion_sequence'] < i
    throat_mask = ip['throat.invasion_sequence'] < i
    sat_p = np.sum(network['pore.volume'][pore_mask])
    sat_t = np.sum(network['throat.volume'][throat_mask])
    sat1 = sat_p + sat_t
    bulk = network['pore.volume'].sum() + network['throat.volume'].sum()
    sat = sat1/bulk
    nwp['pore.occupancy'] = pore_mask
    nwp['throat.occupancy'] = throat_mask
    wp['throat.occupancy'] = 1-throat_mask
    wp['pore.occupancy'] = 1-pore_mask
    return sat


def Rate_calc(network, phase, inlet, outlet, conductance):
    phase.regenerate_models()
    St_p = op.algorithms.StokesFlow(network=network, phase=phase)
    St_p.settings._update({'conductance' : conductance})
    St_p.set_value_BC(pores=inlet, values=1)
    St_p.set_value_BC(pores=outlet, values=0)
    St_p.run()
    val = np.abs(St_p.rate(pores=inlet, mode='group'))
    return val


flow_in = pn.pores('left')
flow_out = pn.pores('right')
model_mp_cond = op.models.physics.multiphase.conduit_conductance
air.add_model(model=model_mp_cond, propname='throat.conduit_hydraulic_conductance',
              throat_conductance='throat.hydraulic_conductance', mode='medium',
regen_mode='deferred')
water.add_model(model=model_mp_cond,
propname='throat.conduit_hydraulic_conductance',
              throat_conductance='throat.hydraulic_conductance', mode='medium',
regen_mode='deferred')

Snwp_num=100
flow_in = pn.pores('left')
flow_out = pn.pores('right')
max_seq = np.max([np.max(ip['pore.invasion_sequence']),
          np.max(ip['throat.invasion_sequence'])])
start = max_seq//Snwp_num
stop = max_seq
step = max_seq//Snwp_num
Snwparr = []
relperm_nwp = []
relperm_wp = []


for i in range(start, stop, step):
    air.regenerate_models()
    water.regenerate_models()
```

```python
    sat = sat_occ_update(network=pn, nwp=air, wp=water, ip=ip, i=i)
    Snwparr.append(sat)
    Rate_abs_nwp = Rate_calc(pn, air, flow_in, flow_out, conductance =
'throat.hydraulic_conductance')
    Rate_abs_wp = Rate_calc(pn, water, flow_in, flow_out, conductance =
'throat.hydraulic_conductance')
    Rate_enwp = Rate_calc(pn, air, flow_in, flow_out, conductance =
'throat.conduit_hydraulic_conductance')
    Rate_ewp = Rate_calc(pn, water, flow_in, flow_out, conductance =
'throat.conduit_hydraulic_conductance')
    relperm_nwp.append(Rate_enwp/Rate_abs_nwp)
    relperm_wp.append(Rate_ewp/Rate_abs_wp)


# Pc curve
hg = op.phase.Mercury(network=pn)
hg['pore.contact_angle'] = 150
hg['throat.contact_angle'] = 150
hg['pore.surface_tension'] = 0.035
hg['throat.surface_tension'] = 0.035
f = op.models.physics.capillary_pressure.washburn
hg.add_model(propname='throat.entry_pressure',
            model=f,
            surface_tension='throat.surface_tension',
            contact_angle='throat.contact_angle',
            diameter='throat.diameter',)
mip = op.algorithms.Drainage(network=pn, phase=hg) # invades froma all sides
mip.set_inlet_BC(pores=pn.pores('left'))
mip.run()
data = mip.pc_curve()
mip.set_outlet_BC(pores=pn.pores('right'), mode='overwrite')
mip.apply_trapping()
data2 = mip.pc_curve()
plt.plot(data.pc, data.snwp, 'b-o', label='without trapping')
plt.plot(data2.pc, data2.snwp, 'r-o', label='with trapping')
plt.xlabel('Capillary Pressure [Pa]')
plt.ylabel('Non-Wetting Phase Saturation')
plt.legend()
plt.savefig("Pc.png", dpi=300)
plt.show()

# Calculating absolute permeability
phase = op.phase.Phase(network=pn)
phase['pore.viscosity']=1.0
phase.add_model_collection(op.models.collections.physics.basic)
phase.regenerate_models()

inlet = pn.pores('left')
outlet = pn.pores('right')
flow = op.algorithms.StokesFlow(network=pn, phase=phase)
flow.set_value_BC(pores=inlet, values=1)
flow.set_value_BC(pores=outlet, values=0)
flow.run()
phase.update(flow.soln)

# NBVAL_IGNORE_OUTPUT
Q = flow.rate(pores=inlet, mode='group')[0]
A = (800*800) * (1.5e-6*1.5e-6)
```

```python
L = (500*1.5e-6)
# K = Q * L * mu / (A * Delta_P) # mu and Delta_P were assumed to be 1.
K = Q * L / A
print(f'The value of K is: {K/0.98e-12*1000:.2f} mD')
```

2. tNavigator input DATA file

```
RUNSPEC

TITLE
Sava-East

DIMENS
50 50 15 /

-- dimensions for equilibration tables
EQLDIMS
1 100 20 1 20 /

TABDIMS
1 1 110 /

WELLDIMS
3 120 1 3 /

CO2STORE
COMPS
 2 /

-- not recognized in OPM
-- FULLIMP

METRIC
UNIFOUT
START
1 'JAN' 2025 /


------------------------------------------------------
GRID
INIT
INCLUDE
'grid.inc' /


------------------------------------------------------
PROPS
CNAMES
'H2O' 'CO2' /

ZMFVD
-- depth  h20  co2  nacl  cacl2
2445 0.99 0.01/

ROCK
```

```
2445 1e-05 /

INCLUDE
'krPorespy.inc'
/

-- density and pvtw: Note that there is no terminating "/" for this
keyword.
-- PVTW
-- p_ref Bw     Cw        VISC
-- -------- ------ ------- ------ ------
--      2445 1.019    2.7E-6 0.370 /

-- surface density
-- works in tNAV, E100, E300 - OPM doesn't accept this in gas-water/CO2Stor
model
DENSITY
--      oil           water          gas
       1000    1000    1.87 /

-- tNAV accepts this only in compositional runs
-- SALINITY
-- -- 1 g/kg = 0.018 mol/g
-- 0.7 /


-------------------------------------------------------
SOLUTION
EQUIL
--      href    p_ref   WOC          Pc@WOC GOC      PcGOC
       2445    240          2000    0            100    0/
/

RTEMPVD
2300    150
2445    155
/


-------------------------------------------------------
SUMMARY

INCLUDE
'summary.inc' /


-------------------------------------------------------
SCHEDULE
RPTSCHED
PRES SGAS WELLS /
RPTRST
BASIC=1 /

WELSPECS
CO2inj Group1 25 25 1* WATER 2* SHUT NO 0 SEG 0/
/

COMPDAT
CO2inj 25 25 1 15 OPEN -1 100 0.3048 /
/
```

```
--Define water and gas injection streams (gas stream is impure CO2)
WELLSTRE
CO2 0.0 1.0 /
/

WINJGAS
CO2inj STREAM CO2 /
/

-- rate 1e6 ~ 0.683 Mtpa
WCONINJE
CO2inj GAS OPEN RATE 1e6 1* 500 /
/

TSTEP
31 28 31 30 31 30 31 31 30 31 30 31
31 28 31 30 31 30 31 31 30 31 30 31
31 28 31 30 31 30 31 31 30 31 30 31
31 28 31 30 31 30 31 31 30 31 30 31
31 28 31 30 31 30 31 31 30 31 30 31
/

TSTEP
15*365.25
/

TSTEP
31 28 31 30 31 30 31 31 30 31 30 31
31 28 31 30 31 30 31 31 30 31 30 31
31 28 31 30 31 30 31 31 30 31 30 31
31 28 31 30 31 30 31 31 30 31 30 31
31 28 31 30 31 30 31 31 30 31 30 31
/

WCONINJE
CO2inj GAS STOP RATE 0 1* 500 /
/

TSTEP
31 28 31 30 31 30 31 31 30 31 30 31
31 28 31 30 31 30 31 31 30 31 30 31
31 28 31 30 31 30 31 31 30 31 30 31
31 28 31 30 31 30 31 31 30 31 30 31
31 28 31 30 31 30 31 31 30 31 30 31
45*365.25
```

OBRAZAC SUSTAVA UPRAVLJANJA KVALITETOM

Nikolina Sušilović, studentica

RJEŠENJE O ODOBRENJU TEME

Na temelju vašeg zahtjeva primljenog pod KLASOM 602-01/23-01/1, URBROJ: 251-70-12-23-1 od 30.01.2023. priopćujemo vam temu diplomskog rada koja glasi:

MULTIPHASE FLOW WITH CO2 AS THE DISPLACING PHASE: DIGITAL ROCK, LABORATORY, AND UPSCALED ANALYSIS

Za mentora ovog diplomskog rada imenuje se u smislu Pravilnika o izradi i obrani diplomskog rada prof. dr. sc. Domagoj Vulin nastavnik Rudarsko-geološko-naftnog-fakulteta Sveučilišta u Zagrebu.

Mentor:

_____
(potpis)

prof. dr. sc. Domagoj Vulin

_____
(titula, ime i prezime)

Predsjednik povjerenstva za
završne i diplomske ispite:

_____
(potpis)

Izv.prof.dr.sc. Luka Perković

_____
(titula, ime i prezime)

Prodekan za nastavu i studente:

_____
(potpis)

Izv.prof.dr.sc. Borivoje Pašić

_____
(titula, ime i prezime)